Detailed study of steady in-cylinder flow and turbulence using stereo-PIV

A master thesis project carried out at SCANIA, Sweden

Julie Vernet

KTH

2012

Abstract

Due to the increase of global warming effects and new legislation in terms of consumption and emissions of engines, it is today of paramount importance to know exactly the flow behavior inside cylinders of engines to be able to improve the combustion process. Until now, at Scania, cylinder heads have been tested in terms of flow coefficient measurements and torque measurements using steady flow rigs. In this project, however, the non-intrusive and optical technique called stereoscopic PIV has been used in order to literally get a 'view' and a better understanding of the flow. An important part of this project has been to study and put into place the PIV setup in order to get the best results from the measurements. Using the stereo technique, the three components of the steady instantaneous velocity in a plane perpendicular to the cylinder axis have been determined. The cylinder and cylinder head were mounted over a device pumping air through the inlet valves reproducing the intake stroke of the engine but with a steady flow. This is useful in order to do different measurements testing several valve lifts and pressure drop in a controlled way. A steady flow is assumed stating that the motion of the valves is slow in comparison to the timescales of the flow. The study of the ensemble averaged flow fields and the turbulence through an analysis of the anisotropic tensor showed an important dependence on the valve lift whereas small dependence is on the pressure drop applied could be noticed indicating that the in-cylinder motion is the same for all engine speeds. The results were then compared to LES simulations and honeycomb measurements and they were in a good agreement.

Résumé

A cause de l'augmentation des effets du réchauffement climatique et des nouvelles législations sur la consommation et les émissions des moteurs, il est aujourd'hui primordial de connaitre avec exactitude le comportement de l'écoulement survenant dans les cylindres des moteurs à combustion afin d'être capable d'améliorer le procédé de combustion. Jusqu'à maintenant, chez Scania, les culasses ont été testées en réalisant des mesures de coefficients de débit et du tourbillon dans le plan perpendiculaire à l'axe du cylindre. Ces mesures étaient réalisées grâce à un dispositif produisant un écoulement permanent à travers la culasse et le cylindre et mesurant le couple exercé sur un plan de nids d'abeille placé en bas du cylindre. Pour ce projet, cependant, la technique optique et non-intrusive PIV a été utilisée afin d'obtenir littéralement une 'vue' et une meilleure compréhension de l'écoulement. Une part importante de ce projet a été d'étudier et de mettre en place l'installation PIV afin d'obtenir les meilleurs résultats à partir des mesures. Grâce à la technique stéréoscopique, les trois composantes de la vitesse instantanée du fluide dans un plan perpendiculaire à l'axe du cylindre ont été mesurées. Le cylindre et la culasse étaient montés sur le même dispositif que les mesures avec les nids d'abeille reproduisant donc la phase d'admission avec un écoulement permanent. Ceci s'est avéré très utile pour réaliser des tests avec différentes ouvertures de valves et différentes différences de pression. L'écoulement peut être supposé permanent puisque le mouvement des valves est lent en comparaison des échelles temporelles en présence dans l'écoulement. L'étude de l'écoulement moyenné ainsi que de la turbulence grâce au tenseur anisotropique ont montré que l'écoulement est fortement dépendent de l'ouverture des valves mais très peu de la différence de pression appliquée indiquant donc que l'écoulement dans le cylindre est le même quelle que soit la vitesse du moteur. Les résultats ont ensuite été comparés aux simulations SGE et mesures réalisées avec les nids d'abeille, les trois techniques donnant dans l'ensemble des résultats similaires.

Acknowledgments

First, I would like to thank my supervisors at Scania, Martin Söder at NMTD and Björn Lindgren at NMTP who gave me the opportunity to work there, entrusted me with this project and helped me any time they were available. I learned a lot thanks to them and this thesis.

Thank you to Hans and Jim for encouraging me during the PIV measurements with their good mood and being available any time I needed technical advices and help. Thank you for being so patient with my Swedish and taught me so much about it.

Special thanks to Daniel Norling at NMPF for spending extensive hours helping me at the 'kanal provrum' and showing so much interest in my project. Problems encountered with the experimental setup seemed less heavy thanks to his support. Thank you to Henrik Dembinski who gave me precious idea for my thesis.

Thank you to Henrik Alfredsson, Ramis Örlü and Sissy Kalpakli from the mechanical department at KTH who took time to answer all my questions about PIV. I would like to thank them for their reactivity and their precious advices anytime I had problems and doubts.

Thank you to my French coordinator Jean-Paul Thibault who provided me precious information any time I asked him and showed me his support from France.

Finally, I would like to acknowledge all the people thanks to whom Scania has been a friendly and pleasant environment to work specially Jörgen, Natalin, Manuel, Patrick, Jonas H., Henrik A., Magnus, Henrik H., Lars, Eric, Hannan, Robert, Fatima, Markus, Catarina, William and Jonas M..

Table of contents

Introduction

I started my engineering studies in France at the engineering school ENSE3 (Ecole Nationale Supérieure de l'Energie, l'Eau et l'Environnement) and then completed my formation with a double degree in Sweden at KTH (Kungliga Tekniska Högskolan). This master thesis has been realized as a part of my double degree.

This project has been carried out at Scania facilities in Södertälje (Sweden). They deliver optimized heavy duty truck, busses, diesel engines and services. The head quarter is in Södertälje but Scania is an international company represented worldwide by approximately 100 national distributors and have production facilities in 7 countries (among them are Sweden, France and Brazil). Scania has more than 35500 employees all over the world. Customer first, respect for the individual and quality are the core values of the company.

The research and development center is located only in Södertälje and employs about 2900 people. The present study has been done as a project at the NMTP group which is a part of the engines research and development department. The 13 people working in this group are responsible for performance of the air inlet system, cylinder head, exhaust-, turbo-, EGR-system, compound, exhaust brake and future gas exchange systems. They simulate and perform engine tests to verify the performance of turbo matches and gas exchange systems. They also test cylinder heads, coolers and pipes using flow rigs.

The project has been realized in collaboration with a PhD student of the NMTD group working on LES simulations using an Open FOAM code. NMTD is responsible for the numerical simulation of fluid flow phenomena within the engine and its intake and exhaust system.

Motivation

For the past 35 years, concern of people about global warming has increased. CO_2 emissions as well as toxic emissions need to be carefully watched and controlled. According to the IEA (INTERNATIONAL ENERGY AGENCY, 2011), in 2009, the sector of transports was responsible for 23% of the worlds Carbone Dioxide (CO_2) emissions and most of them are caused by road transports. The European Union decided to imposed strict limitations on the toxic emissions of road vehicles. This new legislation started with the Euro 1 in 1992, vehicles produced now must respect the Euro 5 legislation and the Euro 6 legislation will come into effect in December 2012. Thanks to the European standards, emissions of Carbone Monoxide (CO), particulates matter or soot (PM), nitrogen oxides (NO_x) and hydrocarbons (THC) have been strongly reduced the last 20 years. Since the decrease in fossil fuels sources, European legislations aim also to replace fossil fuel by bio-fuels. However techniques to produce bio-fuel are not enough evolved nowadays to replace all the fossil fuel. To decrease the engines consumption of fuel is therefore essential.

Improving the combustion process of diesel engines is therefore of paramount importance to decrease fuel consumption and all emissions. To be able to do so it is important to increase the knowledge of air and fuel motion inside engines cylinders and Computational Fluid Dynamic (CFD) is an efficient tool to reach this goal. However, CFD uses models, meshes, numerical schemes and they need to be compared to experimental measurements in order to validate the simulations. A PhD project is currently underway to simulate the in-cylinder flow up till start of injection using LES. The purpose of this project is to simulate the flow field with moving valves and piston. Until now, the only validation has been flow bench measurements of flow coefficient and swirl ratio under steady conditions. The historical reason for using steady flow conditions for measurements of swirl and flow coefficient is that it is assumed that the valves and piston move slowly in comparison to the time scale of the flow. Thus it is assumed that the flow can be considered quasi steady. This assumption has been satisfactorily so far when only first order properties such as the swirl ratio and single cylinder emissions have been considered. No detailed information of the flow field has been available though. Therefore a master thesis project was started to produce experimental data of the detailed flow field under steady flow conditions in a flow bench. Particle Images Velocimetry (PIV) is a non-intrusive technique which is able to give a 'view' of the in-cylinder flow and was therefore chosen as the measurement technique

Objectives

Objectives of the thesis are:

- To set up Stereo-PIV experiments and be able to measure the three components of steady in-cylinder flows.
- To study in-cylinder measurements in terms of dependency to the inlet parameters and give an overview of the turbulence evolution.
- To compare the PIV measurements to CFD simulations and honeycomb measurements.

Layout of the thesis

The first chapter of the thesis treats the theoretical background necessary to understand the study. The equation describing turbulent flows as well as an introduction to some special studies done for these flows are given. Then a part deals with general information about internal combustion engines and the flow bench used in the measurements. A review of previous studies about turbulent and in-cylinder flows has been done and concludes this chapter.

The second chapter is about PIV measurements. It contains information about the experimental setup used in the project. This part can be read independently of the other chapters and seen as a small 'manual' about PIV measurements; advices for settings, processing and useful literature for PIV-related information are given there.

In the third chapter, the results are presented and analyzed. The results are explained for the different cases tested and general conclusion about in-cylinder flows are discussed. Comparison with LES simulations are also summarized in the third part of this chapter.

A final overview of conclusions about the study are drawn in the last part as well as suggestion for future work.

Chapter 1: Theoretical background

1.1. Turbulent flows

Most of the engineering flows are turbulent; it is in general wished for, for their mixing properties. Turbulent flows have the characteristics of being chaotic, unstable and to present a large, three dimensional, range of scales which make them difficult to predict.

The following rules are used in the report to simplify for the reader (except in particular cases):

- Bold characters correspond to vectors.
- The low indexes refer to a component of a vector, that can be Cartesian or polar.
- The high indexes is a reference to a particular instantaneous velocity field and/or the index of the sum in which it is contained.
- The Einstein notation is used, the same index repeated twice implies a sum over all three components

1.1.1. The RANS theory

The two equations that describe the evolution of incompressible flows are the following incompressible Navier-Stokes equations:

$$\frac{\partial u_i}{\partial x_i} = 0$$

$$\rho\left(\frac{\partial u_i}{\partial t} + u_j \frac{\partial u_i}{\partial x_j}\right) = -\frac{\partial p}{\partial x_i} + \mu \frac{\partial u_i}{\partial x_j \partial x_j}$$

with:

- ρ the density of the fluid,
- u_i the i:th velocity component in the x_i direction,
- p the pressure and
- μ the dynamic viscosity of the fluid.

Reynolds Decomposition

The first equation refers to the mass conservation and the second to the momentum conservation, both in the case of incompressible flows. Reynolds suggested a decomposition of turbulent flows in a mean part and a fluctuating part (POPE, 2000):

$$u_i = U_i + u_i'$$

$$p = P + p'$$

where :

- u_i, the instantaneous i-component of the velocity vector,
- U_i, the mean i-component of the velocity vector (mean values are denoted with capital letter or with brackets <>),
- u_i', the fluctuating i-component of the velocity vector.

Capital letters refer to the mean part of the flow and corresponds therefore to a statistical average. This average is realized over a time period and in the case of flow with steady boundary conditions a time-average is the same as a statistical ensemble average realized over N different states:

$$< u >= \boldsymbol{U} = \frac{1}{N}\sum_{i=1}^{N} \boldsymbol{u}^{(i)} \tag{1}$$

When dealing with statistical averages it is often useful to evaluate the standard deviation also called the root mean square (RMS) defined as following:

$$RMS(u_j) = \sqrt{\frac{1}{N}\sum_{i=1}^{N}\left(u_j^{(i)} - U_j^{(i)}\right)^2} \tag{2}$$

RANS equation

When applying the Reynolds decomposition to the Navier-Stokes equations it results in the RANS equations (Reynolds Averaged Navier-Stokes):

$$\frac{\partial U_i}{\partial x_i} = 0; \quad \frac{\partial u_i'}{\partial x_i} = 0$$

$$\rho\left(\frac{\partial U_i}{\partial x_i} + U_j\frac{\partial U_i}{\partial x_j}\right) = -\frac{\partial P}{\partial x_i} + \frac{\partial}{\partial x_j}\left(\mu\frac{\partial U_i}{\partial x_j} - \rho\langle u_i' u_j'\rangle\right)$$

1.1.2. The Reynolds stress tensor

The term $\langle u_i' u_j'\rangle$ refers to the Reynolds stress tensor defined as following in its Cartesian form:

$$\begin{bmatrix} < u_1' u_1' > & < u_1' u_2' > & < u_1' u_3' > \\ < u_1' u_2' > & < u_2' u_2' > & < u_2' u_3' > \\ < u_1' u_3' > & < u_2' u_3' > & < u_3' u_3' > \end{bmatrix}$$

It can be characterized as a stress tensor since its dimension is the same as the one of the viscous stress tensor. Without this term the RANS equations would be exactly the same as the Navier-Stokes equation for the mean part of the flow. All the information about the contribution of the fluctuating part to the momentum transfer is therefore contained in this term.

Turbulent kinetic energy

In particular, the turbulent kinetic energy is defined as the trace of the Reynolds stress tensor:

$$k = \frac{1}{2} < u_i' u_i' >= \frac{1}{2}\sum_{i=1}^{3}\left(RMS(u_i)\right)^2 \tag{3}$$

and corresponds therefore to the mean kinetic energy per unit mass contained in the fluctuating part of the velocity field.

Turbulent anisotropy

Using the Reynolds stress tensor components, the importance of fluctuating velocity in the different directions of the flow can be characterized; this is the study of turbulence anisotropy. A special case is the isotropic turbulence when the fluctuations do not have any directional preference. To realize such a study the invariants of the anisotropy tensor are evaluated (LUMLEY & NEWMANN, 1977):

$$I_1 = b_{kk}$$

$$I_2 = b_{ij}b_{ji}$$

$$I_3 = b_{ij}b_{jk}b_{ki}$$

Where b_{ij} is the normalized anisotropy tensor:

$$b_{ij} = \frac{< u_i' u_j' >}{< u_k' u_k' >} - \frac{1}{3}\delta_{ij} = \frac{< u_i' u_j' >}{2k} - \frac{1}{3}\delta_{ij} \tag{4}$$

And δ_{ij} is the Kronecker operator defined by:

$$\delta_{ij} = \begin{cases} 1, & if\ i = j, \\ 0, & if\ i \neq j, \end{cases}$$

In case of incompressible flows, the first invariant I_1 is always equal to zero and Lumley (LUMLEY, 1978) demonstrated that all the realizable states of turbulence are contained inside a triangle plotted in the plane of the invariants I_2 and I_3, and delimited by the cases of two-component turbulence and axisymmetric turbulence. Limits of the Lumley triangle as well as their meaning are depicted in Figure 1.

This kind of studies have been realized e.g. in (ESCUDIÉ & LINÉ, 2005), (SIMONSEN & KROGSTAD, 2005) and (LAMARQUE, ZOPPÉ, LEBAIGUE, DOLIAS, BERTRAND, & DUCORS, 2010). The size of the triangle or its orientation can vary from a study to another depending if some constants are included in the calculation of the invariants or not but the meaning does not change. The definitions used here are the same than in (PASHTRAPANSKA, JOVANOVIC, LIENHART, & DURST, 2006).

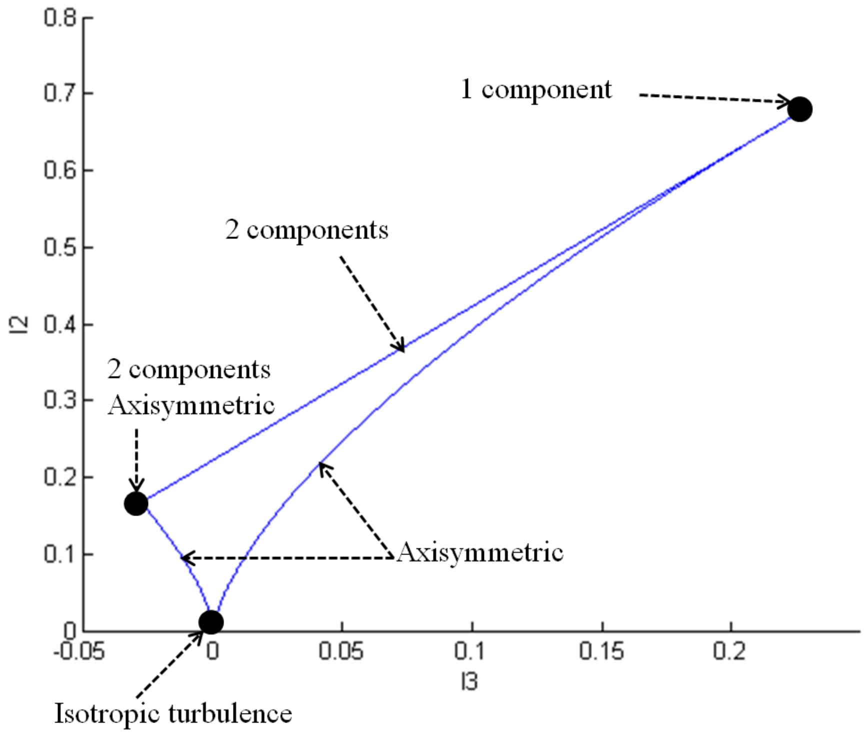

Figure 1. Lumley triangle also called anisotropy-invariant map.

1.1.3. The simulation of turbulent flows

Turbulent flows are composed by a large range of scales depending on the Reynolds number. The simulation of all the scales DNS (Direct Numerical Simulation) gives the closest solution to the reality. Unfortunately today's super computers are still far from capable of calculating DNS of complex flows. Two other choices are then possible. The first choice is RANS simulations, the total Reynolds shear stress is modeled usually assuming isotropic turbulence and only the largest scales of the motion (mean field) is resolved by calculation. This method is fast but a lot of information about the fluctuations is lost. The second option called LES (Large Eddy Simulation) is an intermediate solution.

All the motion scales are responsible for a certain amount of turbulent kinetic energy; the smallest scale called the Kolmogorov scale contains the smallest amount and the largest scales contain a larger amount of energy. A length scale threshold value has to be defined; all the scales smaller than this limit will be modeled and the resolution of the Navier-Stokes equation will be made only for larger motion scales. The precision of the results is therefore higher when using the LES method than the RANS method if enough scales has been resolved.

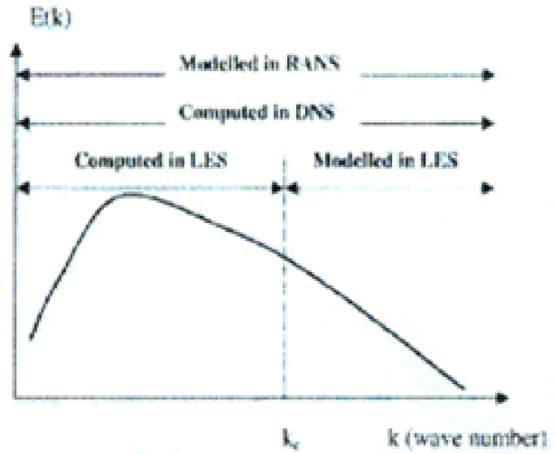

Figure 2. Turbulent energy spectrum plotted as a function of wave number.

1.2. Internal combustion engines

Heat engines convert chemical energy from combustion of fuel into work. They can be classified into two categories:

- External combustion engines for which the fuel-air mixture is separated from the working fluid. It means that the combustion occurs in one part of the engine and then the rise in heat is transmitted to the working fluid through an interface. Stirling and steam engines are examples of external combustion engines.
- Internal combustion engines are the ones of interest in this study. There is no interface separating the air-fuel mixture to the working fluid which is directly the product of the combustion.

The internal combustion engines can also be classified depending on the method used to ignite the combustion of the fuel-air mixture; they can be either Spark-Ignited (SI) engines or Compression-Ignited (CI) engines. The SI engines are also called Otto engines; the fuel is mixed with the air and a spark is at the origin of the combustion. The engines of interest here are the CI engines or Diesel engines for which it is the compression of the air implying a raise of pressure and temperature of the gas and thus triggers the combustion.

The engines produced by Scania are qualified as four-stroke reciprocating CI engines. That means that the working fluid will produce a movement of translation then transformed to a rotational movement using a mechanism composed of a piston, a rod and a crank. One cycle is composed of four strokes described below and in Figure 3. Two-stroke engines are also produced but not by Scania, a description of their mechanism can be seen in e.g. (HEYWOOD, 1988).

1.2.1. Four-strokes CI engines

In order to describe the mechanism of the four strokes, one first needs to define terms commonly used in the context of piston-engines. The strokes of the piston is from the bottom dead center (BDC), for which the volume within the cylinder is maximal, to the top dead center (TDC) which corresponds to the minimal volume in the cylinder. The ratio of these maximal to minimal volumes is called the geometric compression ratio.

The mechanism of the four strokes is described in Figure 3 and the valve timing process in Figure 4:

- During the intake stroke, intake valves open and air enters into the cylinder when the piston goes from TDC to BDC.
- Then the compression stroke occurs. The intake valves close and, going back to the TDC, the piston compresses the air rising its pressure and temperature above the auto-ignition temperature of the fuel injected at the end of this stroke. The combustion starts increasing even more pressure and temperature.
- The power or expansion stroke is when this increase in pressure pushes the piston back to the BDC. The pressure continues to increase due to the combustion even when it already started to push down the piston.
- Once the piston is at the BDC, the exhaust valves are opened, the piston goes from the BDC to the TDC to evacuate the products of the combustion; this is the exhaust stroke.

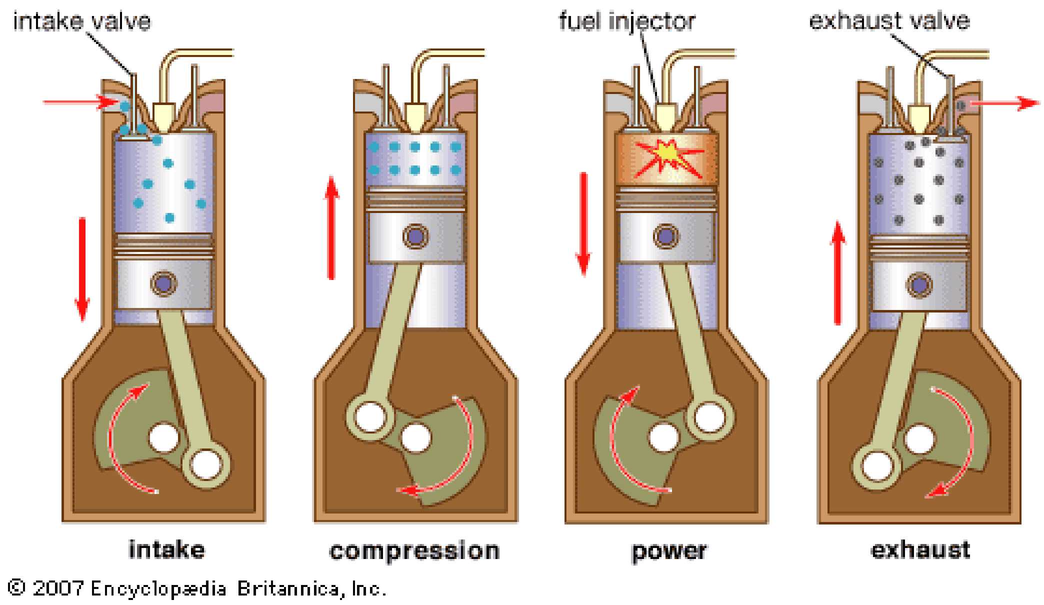

Figure 3. The different phases of a four-stroke Diesel engine (Four-stroke diesel engine).

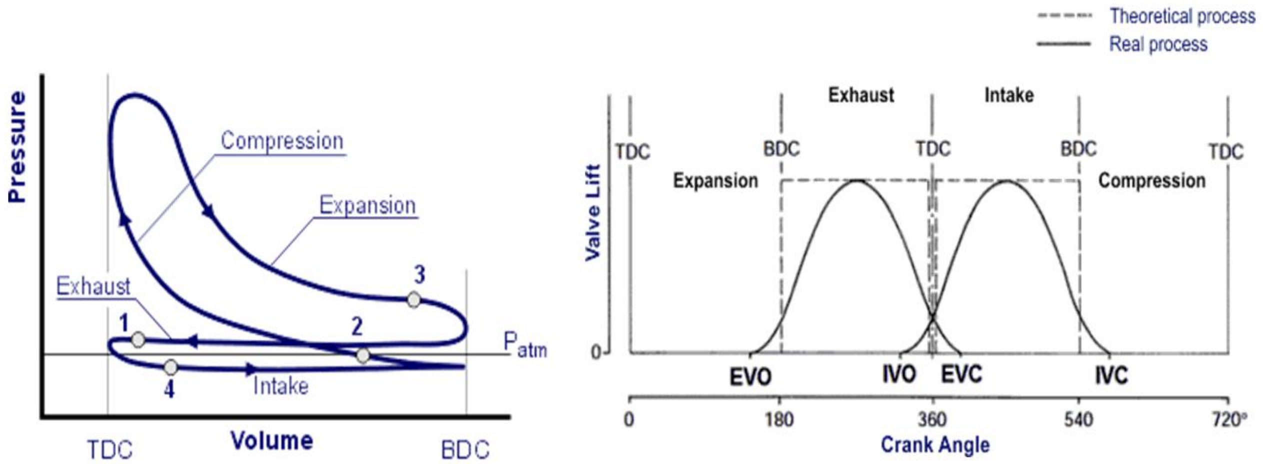

Figure 4 To the left, Pressure/Volume diagram of diesel cycle. To the right theoretical and real valve timing process in 4-stroke cycle (Diesel Engine Fundamentals).

1.2.2. The fuel/air mixture

The fuel is injected into the cylinder using the fuel injector at the end of the compression stroke. Because of the high pressure in the fuel and high pressure and temperature of the compressed air, the liquid fuel atomizes into small droplets and the combustion starts almost immediately. The short delay between the injection and the beginning of the increase in temperature due to the combustion is called the ignition delay. This phase is of paramount importance for the improvement of the engines in terms of reducing the consumption of fuel and the emissions since the way the fuel mixes with the air during the ignition delay has a direct effect on the combustion efficiency (ARGACHOY & PIMENTA, 2005).

It is well known now that the design of intake ports and valves as well as the number of them used to introduce the air into the cylinder during the intake stroke has an effect on the in-cylinder air motion which has itself a repercussion on the fuel/air mixing at the end of the compression stroke.

Actually to improve the mixing process, the ports and valves are usually designed in order to induce a swirl and a tumble motion in the air during the intake stroke. The swirl characterizes a rotating motion induced in the plane perpendicular to the cylinder axis whereas the tumble is a rotating motion in the plan parallel to the cylinder axis. The swirl will be conserved during the compression stroke whereas the tumble will break down into smaller scales increasing the level of turbulence of the compressed air. Due to the swirl motion, the fuel injected in the cylinder will travel a longer distance before hitting the wall and the increase in turbulence level will improve the fuel/air mixing. The in-cylinder mixing process is also improved thanks to both the swirl and the tumble, reducing the inhomogeneities such as pockets of exhaust gases. However, the swirl and the tumble motion need to be known and studied in detail since they can also have negative effects on the combustion process; a too high swirl may lead to the fuel sprays collide which drastically increases the local air/fuel ratio, increasing soot emissions and fuel consumption.

In order to characterize the swirl motion, a swirl ratio can be calculated evaluating the angular momentum of the air around the cylinder axis (z-axis) equal to:

$$M_z = \int \rho \, (\boldsymbol{v} \times \boldsymbol{r}) \boldsymbol{n} U_z dA$$

Where:

- ρ is the density of air

- $\boldsymbol{u}$ is the velocity vector
- $\boldsymbol{r}$ is the radial vector
- $\boldsymbol{n}$ is the normal vector to the surface (vector element of the cylinder axis)
- U_z is the velocity in the direction of the cylinder axis
- dA is the surface element

If the values are discrete, the integral can be transformed in a sum operator and the following equation applies:

$$M_z = \sum_{i=1}^{K} \rho^{(i)}\left(\boldsymbol{u}^{(i)} \times \boldsymbol{r}^{(i)}\right)\boldsymbol{n}^{(i)} U_z^{(i)} \Delta A^{(i)} \tag{5}$$

Where K is the number of discrete values or elements and $\Delta A^{(i)}$ is the element surface. Then the Swirl Ratio (SR) is calculated with:

$$SR = \frac{2\,\rho\,S\,M_z}{q_m^2} \tag{6}$$

With, S the stroke of the piston and q_m the mass flow.

This SR can be calculated for different valve lifts and then a weighted averaged can be made over the different values in order to characterize a mean SR for the engine.

1.2.3. Measuring the swirl using a steady flow bench

The test bench used in the experiments is designed for intake or exhaust port flow measurements (see Figure 5) . Here, only the intake port flow setup is considered. The rig consists of two settling chambers with a displacement pump flow measurement device in between. On top of the upstream settling chamber there is the honeycomb torque measurement device and the liner. The cylinder head is positioned on top of the liner. On top of the cylinder head there is the valve adjustment mechanism. On the inlet of the intake ports there is a plate with 10 mm radius allowing for a smooth inlet flow condition. On top of the downstream settling chamber there is a pipe with a T-junction. One end of the T-junction is connected to the fan and another to the atmosphere through a throttle. The throttle regulates the flow rate through the cylinder head.

The standard measurement equipment measures the total pressure drop between the inlet atmosphere and the upstream settling chamber, the torque on the honeycomb, using a strain gage at the end of an arm connected to the honeycomb at the liner centre, and the flow rate. The temperature in the upstream settling chamber and the atmospheric pressure is also measured. The flow rate is proportional to the speed of the displacement pump at zero pressure drop between the settling chambers.

The operator controls the valve mechanism to a fixed valve lift and then adjusts the throttle and the speed of the displacement pump to achieve a steady state condition with zero pressure drop across the displacement pump and the desired pressure drop between atmosphere and the upstream settling chamber. The swirl ratio and the flow coefficient is then calculated using the measured data. For further information see (LINDGREN, 2004)and (LINDGREN, 2003).

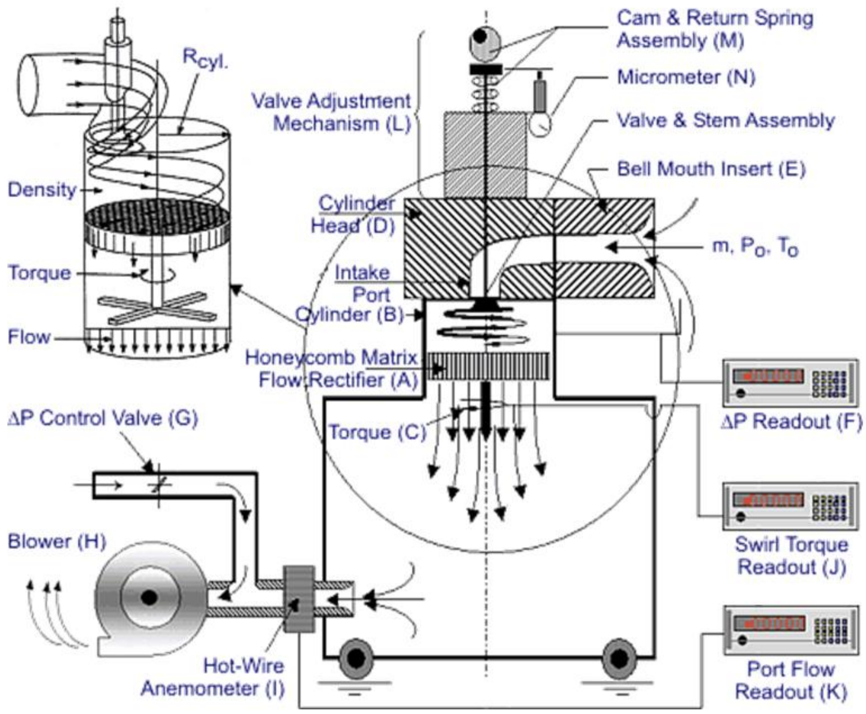

Figure 5. Intake port flow and swirl bench (Valves and Ports in Four-Stroke Engines).

1.3. Previous studies

Understanding of the in-cylinder flow field is indispensable to reduce the fuel consumption and the emissions of engines. As explained earlier, the swirl and the tumble are actors of this improvement. Simulations are conducted to be able to better understand the flow interactions from the intake stroke until the exhaust stroke and understand the effect of the piston, valves and port designs on the flow field. However, in-cylinder flows are turbulent. As explained in the turbulence part, all the scales of turbulent flows cannot be simulated since it is too time consuming. In the best case, one can simulate them using LES and by modeling only small scales below a certain threshold length. That means that experimental studies are still needed first for comparison and then to give information about the best model that should be used for the simulations.

In-cylinder flow experiments have been strongly improved with the use of optical diagnostic techniques, first the LDV (Laser Doppler Velocimetry) and then the PIV (Particle Images Velocimetry). (REUS, ADRIAN, LANDRETH, FRENCH, & FANSLER, 1989) realized one of the first PIV investigation of in-cylinder flows. The PIV is nowadays commonly used to study the tumble motion in the plane parallel to the cylinder axis like in (MURALI KRISHNA & MALLIKARJUNA, 2011). E.g. in (KEROMNES, DUJOL, & GUIBERT, 2010), PIV measurement has been used to study the effect of different valve geometries on the tumble motion during the intake and compression strokes of the engine. Conclusion about the impact of these different geometries on the fluctuating part of the velocity field could been drawn using this technique.

An important amount of studies of the swirl motion of the flow have also been made with the PIV technique e.g. (NORDGREN, HILDINGSSON, JOHANSSON, DAHLÉN, & KONSTANZER, 2003), (COSADIA, BORÉE, CHARNAY, & DUMONT, 2006), (HEIM & GHANDHI, 2011) and (ALGER, MCGEE, GALLANT, & WOLLDRIDGE, 2004).

In (HEIM & GHANDHI, 2011), PIV measurements have been made studying two different designs for the inlet valves. Results for the two components of the velocity in the plane perpendicular to the cylinder axis were in good agreement with solid body rotation. They also showed that the center of the solid body rotation could not be confused with the center of the cylinder and that the location of the center does not really vary with the engine speed. This PIV study, as many others e.g. (COSADIA, BORÉE, CHARNAY, & DUMONT, 2006) have been realized with motored engines in order to study the cycle-to-cycle variations and the engine speed effects.

In (NORDGREN, HILDINGSSON, JOHANSSON, DAHLÉN, & KONSTANZER, 2003), authors compared PIV measurements made also on a single cylinder motored heavy duty diesel engine using a transparent piston to be able to take the picture from the bottom of the cylinder. Results have been compared to CFD simulations and honeycomb measurements of the torque and therefore swirl ratio. The engine speed was there constant and only the cycle-to-cycle variations during the intake and compression strokes have been investigated. Results were in good agreement with the simulations and showed that the cycle-to-cycle variations were more important for some crank angles than others. However, differences were clearly visible between the swirl ratio measured with the honeycomb and the swirl ratio evaluated with the PIV technique and the authors concluded that it is due to the loss of information of PIV for which the out-of-plane component of the velocity could not be evaluated.

Finally, since the PIV cannot be used when too much light is in the field of view a technique called Combustion Image Velocimetry (CIV) has been used in (DEMBINSKI, 2011) in order to study the flow motion during the in-cylinder combustion process and the effects of the swirl motion and the injection pressure of the fuel on the mixing process. This technique is similar to the PIV but instead of using a laser lighting up some droplets, the soot were directly used as particles. This study has been made by a PhD student at Scania and showed interesting results on the effects of the swirl on the combustion process like the fact that the solid body rotation could not be observed anymore at the end of the injection. The author also showed that the swirl motion is not centered with the cylinder and that the increase in vorticity increase the mixing process. The pressure injection of the fuel has also been studied there and showed to influence the flow field quite considerably.

Chapter 2: PIV measurement technique

2.1. Introduction and PIV principle

Particle Image Velocimetry (PIV) is a method used to get the instantaneous velocity components of the flow in a wide domain. It is an optical method using laser and one or more cameras linked to advanced software used to do the acquisition and the processing of the data.

This makes it possible to observe the flow and get velocity components in a plane and not only in one single point, without being intrusive as the case with methods using probes like the hot-wire anemometry method.

Different types of PIV methods have been developed depending on what is needed to be observed; classic PIV, to get the two components of the velocity in a two dimensional domain, is the most common. Micro PIV in order to observe fluids in micro channels or even in droplets are also used. Stereoscopic PIV (S-PIV) or PIV techniques like the tomographic PIV make it possible to include the third component of the velocity in the results. During this project, stereoscopic PIV has been used to observe and evaluate the three components of the instantaneous velocity in a horizontal plane of an engine cylinder.

2.1.1. PIV evaluation

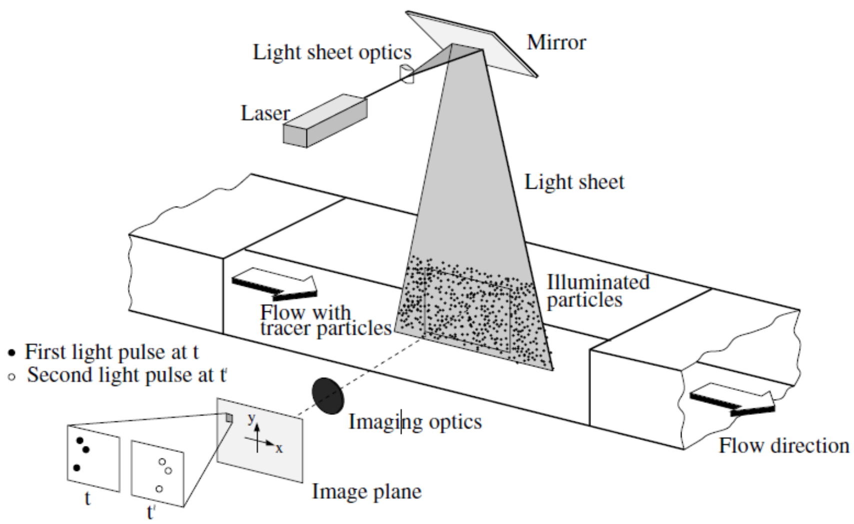

Figure 6. Principle of Particle Image Velocimetry. The camera takes one frame of each laser pulse, **the first one at time t and the second one at time t'=t+Δt.** (RAFFEL, WILLER, WERELEY, & KOMPENHANS, 2007)

With classic PIV, the two components of the velocity in a two-dimensional domain can be observed. In order to be able to see the flow, particles are injected as tracers. A thin laser sheet lights up the plane or area of interest as well as the particles present and one camera takes pictures of these illuminated particles seeding the flow.

The laser is actually constituted of two lasers organized with mirrors in order to produce exactly the same beam at the same position and it is able to produce two pulses (one from each laser component) with a short interval time Δt (cf. Figure 6). A correlation algorithm is used to determine the distance covered by the particles between the first and the second laser pulse, Δs. Thanks to this information and the known time interval between the laser pulses, the two components of the instantaneous velocity of the particles can be determined.

Two different types of PIV evaluations are possible. The first option is to take only one frame exposed two times ; the first time by the first laser pulse at time t and the second time by the second laser pulse at time t', and evaluate the PIV using an auto-correlation method. This technique was often used in the past because the cameras were not fast enough to take two frames with a sufficient small Δt. The problem of this method is that it is not possible to know which particles on the frame come from the first exposure and which ones come from the second thus the direction of the displacement is not available. The second technique is the one described in Figure 6; to take one frame for each laser pulse and then evaluate the PIV using cross-correlation between the different frames, it is the method used the most nowadays.

Description of the cross-correlation mechanism

The principle of the PIV evaluation is described in Figure 7 and Figure 8. In the first step, the couple of frames is subdivided into small interrogation windows with few pixels, and then the aim of the cross-correlation algorithm is to evaluate the light intensity shift. The cross-correlation algorithm will work with each couple of interrogation windows; it will determine the relative displacement needed between the two interrogation windows of the couple to match the intensity repartition on them. The accurate relative displacement between the windows will correspond to the highest value of the correlation function which is also called the correlation peak.

To study the correlation map after processing the images is a good option to evaluate the results and the correlation process, as will be shown later.

Mathematical background

The theory of correlation applied in PIV is actually a statistical method close to the ones used in signal analysis. The two-dimensional cross-correlation used for this kind of analysis is:

$$R(\Delta x, \Delta y) = \int_{-\infty}^{+\infty} \int_{-\infty}^{+\infty} F(x, y) G(x - \Delta x, y - \Delta y)\, dx\, dy$$

Where F and G are the signal functions.

In the case of PIV evaluation the signal is the light intensity field. The images, as well as the interrogation windows, are constituted of pixels. So taking a couple of windows of size MxN pixels, like in Figure 7, each pixels has a certain position in the image and a certain amount of light. For example the intensity of the pixel at the position (n,m) in studied window of frame a (at time t) is (Figure 7):

$$I_a(n, m)$$

The cross-correlation, in a discrete form, used for the PIV evaluation is:

$$R(k, l) = \sum_{m=0}^{M} \sum_{n=0}^{N} I_a(m, n)\, I_b(m - k, n - l)$$

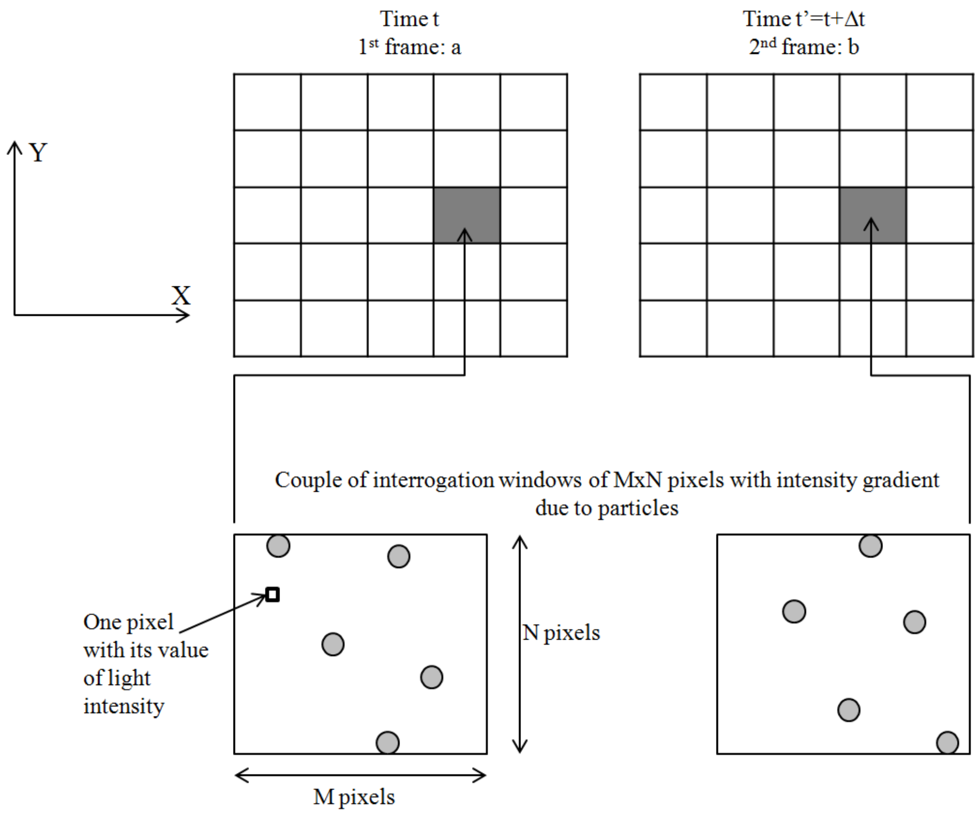

Figure 7. Subdivision of the frames in interrogation windows. In this case 25 windows and no overlapping between them. The grey dots represent the particles.

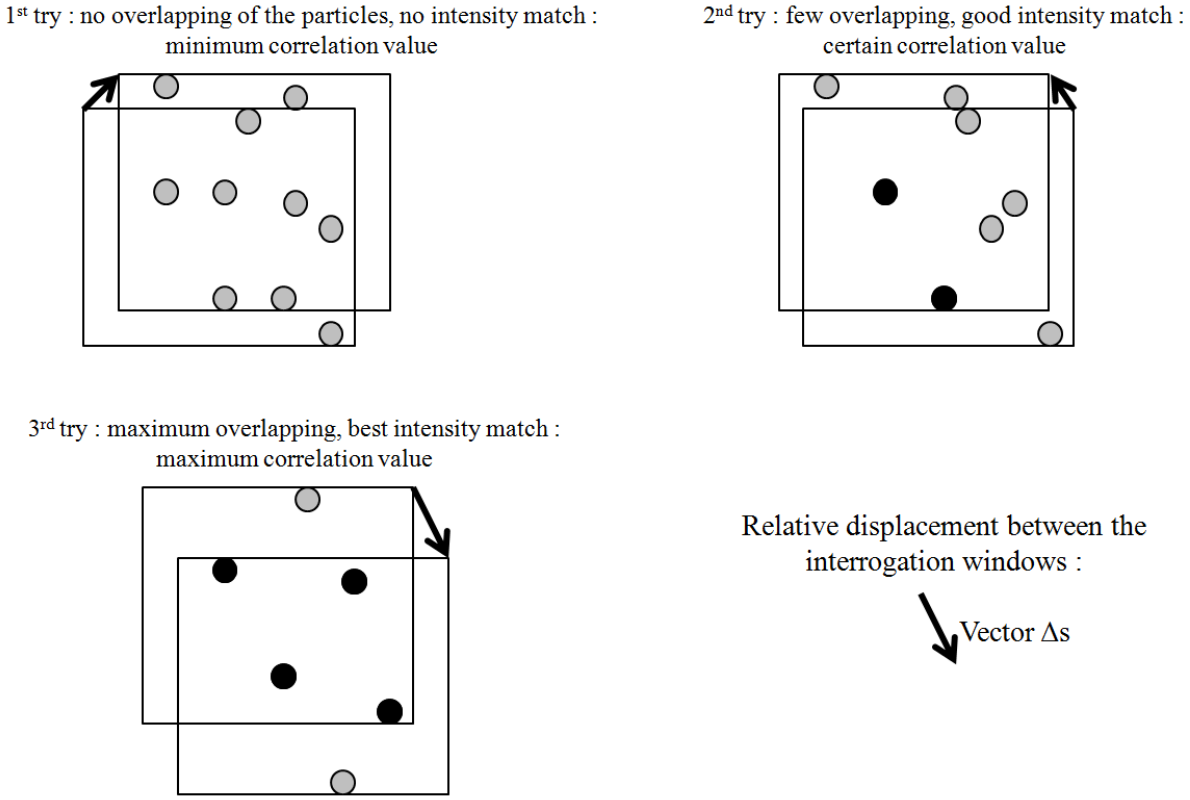

Figure 8. Principle of the cross-correlation algorithm to find the intensity shift between the two frames and deduce the instantaneous velocity of the particles. The grey dots represent the particles on one frame at a time and the black dots are the particles present on the both frames and so overlapping for the applied relative displacement of the interrogation windows.

The value of k and l for which the function R get its maximum (correlation peak) correspond to the optimal relative displacement between the two interrogation windows in terms of pixels. Thanks to a calibration step, explained later, the displacement in pixels can be evaluated as a distance and the vector velocity deduced from:

$$v = \frac{\Delta s}{\Delta t}$$

This method gives the two dimensional instantaneous velocity vector for each couple of interrogation windows and not for each particle contained within so it is a statistical method based on the assumption that the displacement of all particles in the same window is homogeneous, if particles go in different directions and the velocity range is too large, the intensity pattern is not conserved between the two frames and the cross-correlation process cannot be used successfully. Applying this process to all the interrogation windows couples of the images will give the two dimensional instantaneous velocity field in the surface.

It is commonly thought that the PIV algorithm tries to follow each particles between the two frames and determines the instantaneous velocity in that way. It is not the process used by PIV but it is an existent technique which is called Particle Tracking Velocimetry; the mean difference being that the number of particles per pixel needs to be much smaller in the case of PTV.

2.1.2. Stereoscopic PIV, SPIV or 3D-PIV

The stereoscopic PIV also called 3D-PIV or S-PIV is a PIV technique for which the three components of the flow's instantaneous velocity can be obtained. This technique is quasi three dimensional since the three components are observed only in the plan aligned with the laser sheet and not in a volume. To realize S-PIV measurements, one more camera is needed. Classic configurations can be seen in Figure 9. For classical PIV the camera is usually perpendicular to the laser sheet to get the most accurate results, in the case of S-PIV it is not the case anymore.

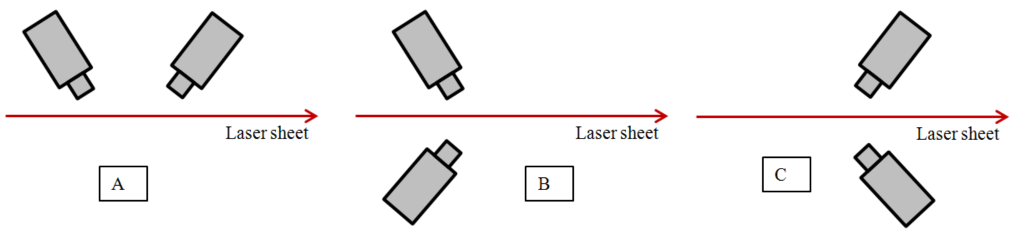

Figure 9. Three different configurations for the cameras when using S-PIV

Three different configurations are recommended for the arrangement of the cameras (Figure 9); in the configuration A the cameras are placed backward and forward from the laser sheet direction and so do not get the same amount of light (see the paragraph about the particles); arrangements with the aperture of one of the camera is needed to correct this difference. In configuration B and C the cameras are respectively placed both backward and forward from the laser sheet direction and therefore get the same amount of light. It will be explained later that the configuration C is actually the best one because the light intensity reflected by the particles in the forward direction is superior to the one in the backward direction. For the same reason the distance from the laser sheet to the lenses of the cameras should be of the same order to get the same amount of light.

The Scheimpflug criterion

Using S-PIV, Scheimpflug adaptors are needed when the object plan is no longer parallel to the lens plane (as is the case when the cameras are not perpendicular to the laser sheet), to get the entire image plane focused. The tangent to the lens plane should intersect exactly at the same point as the tangents from the image plane and the object plane as can be seen in Figure 10 (PRASAD, 2000),(LAVISION GmbH, 2010). Scheimpflug rings or adaptors are used to rotate the image plane in order to get the coincidence between the three tangents.

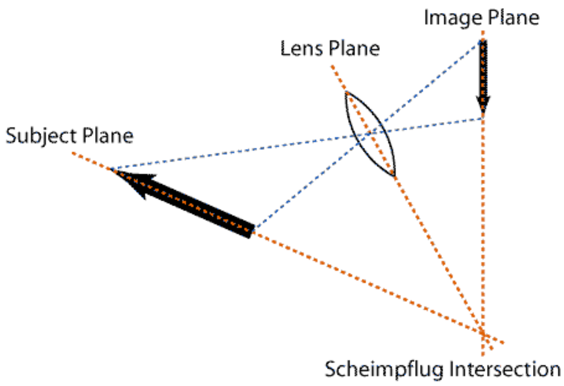

Figure 10. Condition to respect the Scheimpflug principle (Scheimpflug principle).

The S-PIV reconstruction mechanism

The S-PIV process uses the same recording method as the simple PIV; each camera will take two frames with a defined interval time. The cameras need to be perfectly synchronized because both frames must be taken exactly at the same time to capture the same particles and get the third component of the velocity. When dealing with one picture or one image, the cameras take actually 4 frames. For example, a set of 100 pictures contains 400 frames.

Then techniques from the PIV process and the ones used by human eyes and brain are very similar in order to get the three components of the instantaneous velocity. Indeed, it can easily be noticed that if we hide one of our eyes we are still able to see correctly movements but we can’t really appreciate distances towards and away from us; our eyes take two dimensional images and our brain is able to do a three dimensional analysis similar to the one the PIV software does.

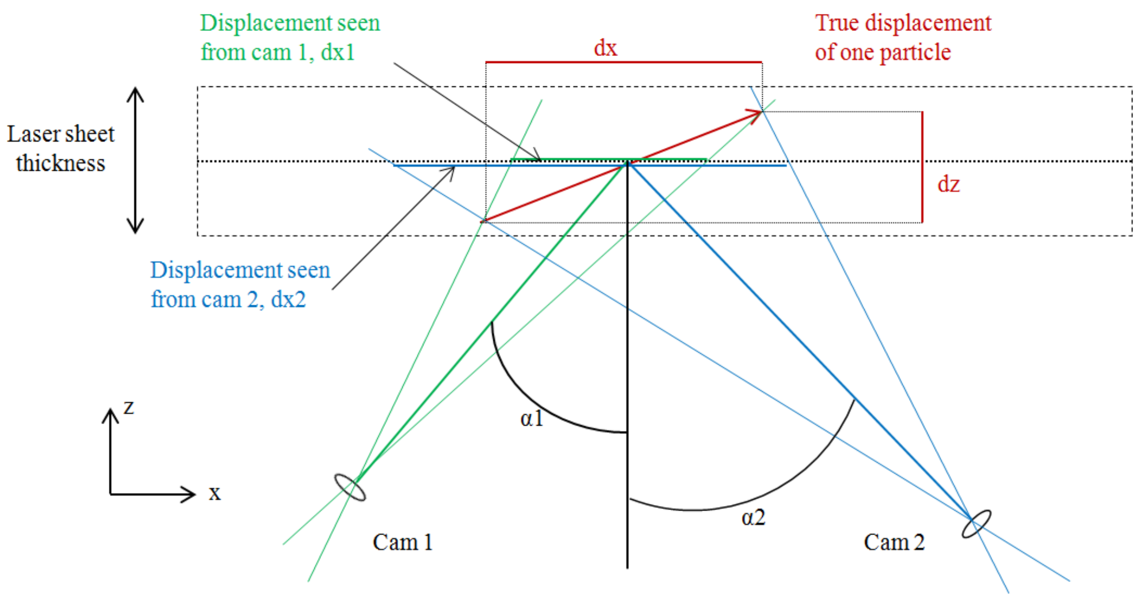

Figure 11. Principle of Stereoscopic Particle Image Velocimetry

The software realizes the PIV evaluation for the images of each camera; this process gives the displacements found by each camera in the two directions of the plane (dx_1, dy_1, dx_2, dy_2, the indices refer to cameras 1 and 2 respectively). Then the final displacements dx, dy (in-plane displacement) and dz (out-plane displacement) are determined using the following relations, (FEI & MERZKIRCH, 2004),(RAFFEL, WILLER, WERELEY, & KOMPENHANS, 2007) , (the notations are visible in Figure 11):

$$\begin{cases} dx = \dfrac{dx_2 \tan\alpha_1 - dx_1 \tan\alpha_2}{\tan\alpha_1 - \tan\alpha_2} \\ dy = \dfrac{1}{2}(dy_1 + dy_2) \\ dz = \dfrac{dx_1 - dx_2}{\tan\alpha_1 - \tan\alpha_2} \end{cases}$$

Several options are available for the acquisition of the images like the choice of the number of recorded pictures, the interval time between them etc, these options are controlled by the user through the software. Then, different processing plans can be applied to get accurate results. The following parts of this chapter will provide information about the PIV arrangements used for this project and general advices which could be starting points for further PIV or S-PIV measurements.

2.2. Settings and recording of the images

The most important and difficult part when using PIV measurements is to install all the equipment, cameras, laser and others, and to set recording parameters to be able to get pictures giving accurate results. Some conditions need to be respected in order not to induce large errors during the evaluation.

2.2.1. Installation and material used

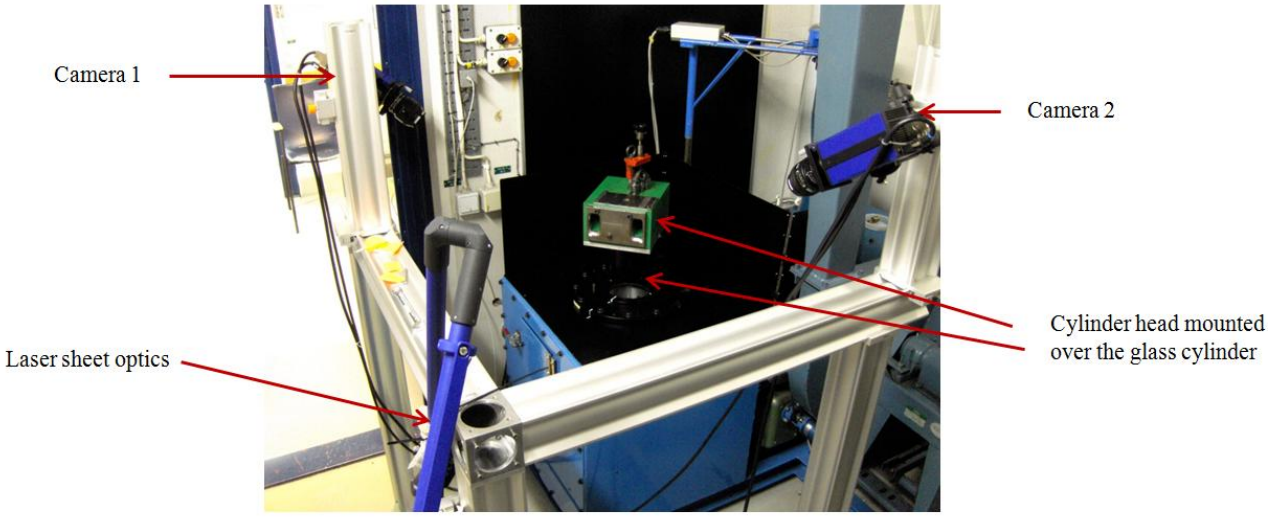

Figure 12. Configuration of cameras and laser sheet optics around the ensemble head cylinder-cylinder to take S-PIV measurements in a horizontal plane of the cylinder.

As explained in the introduction, the aim of this project is to study the flow fields and the swirl motion which occurs in horizontal planes of the cylinder. The ensemble cylinder head and cylinder is mounted over a fan which pumps out the flow coming through the inlet valves and therefore reproducing the inlet stroke of a engine. A glass cylinder is used to make possible it to take pictures through its wall. The final configuration can be seen in Figure 12. Only few positions of cameras were possible because of the size of the cylinder head and the fan. This one was the best one since it gives better results if both cameras are locking toward the same direction. An angle of about 90 degrees between them with a symmetrical disposition compared to the axis perpendicular to the laser sheet ($\alpha_1 = \alpha_2 = 45°$ in Figure 11) is also known to handle more accurate PIV evaluations (PRASAD, 2000). The angle here is a bit larger because the field of view was obstructed by the cylinder head if the cameras were too close to each other.

Cameras

Cameras used for this project are CCD cameras (Charge Coupled Device) called Image Pro X 4M (LAVISION GmbH, 2011). They have the advantages of a large optical aperture and a high dynamic range. The dynamic range of cameras correspond to the ratio between the maximum and the minimum intensity of light that cameras are able to measure and is therefore really important in the case of PIV measurements. The ones acquired by Scania have a dynamic range of 14 bits and a high spatial resolution of 2048×2048 pixels. These cameras are known to be slow with a frequency up to 14Hz (they cannot acquire more than 14 pictures per second). CMOS cameras have been developed with a much faster recording frequency (more than 1000Hz) and are used for time-resolved PIV. However the quality of the recordings is inferior to the one of the CCD cameras because their sensors have an inhomogeneous sensitivity and produces more noise (Cf. particles intensity part). The choice of CCD cameras to study non-time dependant flows like for this configuration is therefore relevant.

The lenses of the cameras were mounted on Scheimpflug adaptors in order to get focus on the horizontal plane.

Laser

Lasers used for most of PIV measurements are called Nd:YAG lasers and produce a green beam with a wavelength of 532nm. This kind of laser is classified level 4 because they are really powerful and need to be used carefully with protective goggles. The pulse energy of the one used at Scania is up to 200mJ. It is a double-cavity laser because, as explained earlier, two lasers are actually contained to produce a total repetition rate up to 15Hz. The produced beam is brought from the box containing pump chambers and Q-switches components up to a light sheet optic thanks to an arm visible in blue in Figure 12.

The user must verify that these two laser beams are perfectly overlapping over the surface of interest. This can be done taking two frames with a really short interval time (only 1 or 2μs). The particles of each frame are illuminated by a different laser beam and the PIV evaluation should therefore give a really small displacement if they are overlapping correctly. If it is not the case, it is possible to open the laser box and adjust the mirrors contained within to correct it. For more information on how to adjust laser beams see (LAVISION GmbH, 2011).

A laser sheet thinner than 2mm was used for measurements, this thickness is the same all over the plane.

Hardware and Software

To run the PIV process and analyze the results, the version 8.0 of the software DaVis has been used and results have been exported to Matlab. This software is able to run PIV for a lot of different configuration, even if cameras and laser are not PIV ones, the only thing it needs is good quality pictures with particles. For example it has been used to process pictures of soot particles in the study of (DEMBINSKI, 2011).

This software is installed on a computer with a GPU (Graphic Processing Unit). This is needed to acquire the frames and record them with a high enough speed but it can also be used to run the S-PIV evaluation. Calculations are approximately ten times faster when using GPU than a regular CPU (Central Processing Unit). However the implemented code in the software to run the PIV is not the same if the process occurs on the CPU or on the GPU. Options available for the evaluation are not the same in the two cases. Most of the time in this study, due to the number of pictures recorded, the process has be made using the GPU'.

2.2.2. Seeding particles

The size of the particles used to seed the flow depends on its physical properties. For air flows, like in this project, droplets (smoke made with oil or alcohol like in this project) with a diameter about 1 to 5 µm are commonly used but for water that would be solid polystyrene or polyamide spheres in the range of 50 to 100 µm. The density of oil is obviously higher than the air density so it is important that the particles are small enough to be able to follow the flow correctly.

Particle images size and density

An important parameter when using PIV evaluation is the size of the particle images meaning the size in number of pixels that particles cover on pictures. That can obviously vary with the physical size of the particles but also with the focus of the cameras by variation of their aperture or f-number (f#) (a large aperture corresponds to small f#). Decreasing the aperture, and so increasing the f#, increases the depth of focus and therefore the size of particles on images. For this project, the f# of each cameras were equal to 1.8.

Too large particle images can overlap easily and induce noise in the pictures but too small particles will induce a consequent error called peak locking error due to weakness of the sub-pixel estimator of the PIV. Actually, when the PIV process occurs, if the particle images are small, the correspondent correlation peak will be really sharp; only one or two pixels large. This is due to the fact that the overlapping of the particles for the couple of interrogation windows is only possible for an exact displacement. The position of the maximum of the correlation function will therefore be known with a precision of one pixel. On the other hand, if the particles images are of order of 3 pixels, the correlation peak is spread over several pixels and a Gaussian interpolation can be made on the shape of the peak; the maximum can therefore be approximated with a better precision (inferior to one pixel), this is the sub-pixel estimator.

The precision of the sub-pixel estimator can be estimated thanks to the probability density function given by Davis. Indeed this function handles the number of particle images over the range of pixels displacements. Three different functions are suggested; the best choice to evaluate the sub-pixel estimator is to chose 'V.mod 1' in the pdf settings. This option gives the distribution of the particle images displacements cutting-off their integer value, they are plotted in function of their decimals only. It can be seen in Figure 13, that when the particle images are too small all the values of pixels displacement are biased toward the integer values, this is called the peak-locking effect. For particle images large enough the distribution is more homogeneous; the sub-pixel estimator has been able to estimate displacements with at least a precision of one tenth of a pixel.

The error due to a weak sub-pixel estimator is called the peak-locking error and can be read in the settings of the pdf menu (DaVis). This is a necessary method to judge PIV results. For example, in Figure 14, the PIV-evaluation giving the pdf to the left handles a peak-locking error of 0.245 instead of only 0.015 to the right. It says actually that even if the shape of the pdf on the left is saying that the sub-pixel estimator is not efficient, it is not that bad. Indeed the peak-locking error is always contained in the range 0-1 with 0 for really efficient sub-pixel estimators and 1 for poor estimators.

However, it has been shown that the peak-locking error does not affect the mean velocity if the average is made on an efficiently large sample of instantaneous velocity fields, even in the case of absolute peak-locking error (equal to 1) (CHRISTENSEN, 2004). The lack of precision of results influences only the estimation of turbulent fluctuations and so RMS values.

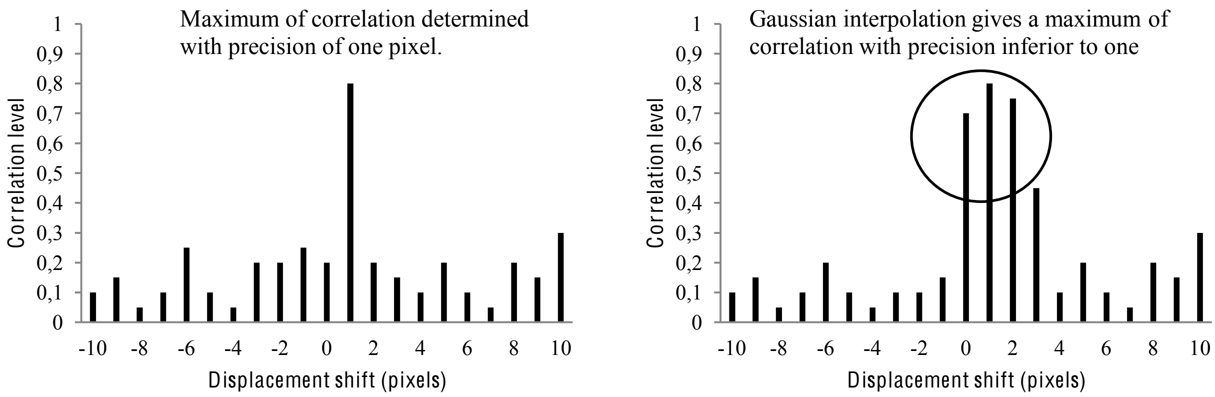

Figure 13. Comparison of the correlation results for particle images sizes inferior to one pixels(left) and particle images sizes between 2 and 4 pixels (right).

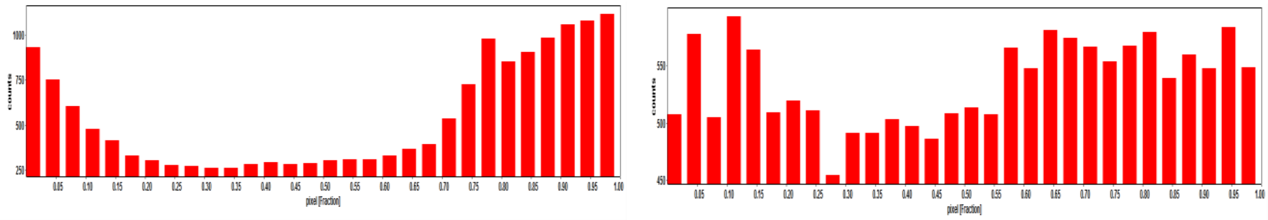

Figure 14. Distribution of the particle images displacements over their first decimal evaluated. On the left, particle images too small and displacement evaluated biased to integer values. On the right, particle images large enough to get evaluation of displacements with one tenth precision.

The density of particle images in the interrogation windows should also be controlled. Here again an equilibrium is necessary; too many particles can induce noise and not enough particles would decrease the resolution. It is common to talk about a particle image pair because it corresponds to a particle image that is present in the interrogation window of both the first and the second frame. It will be explained later that particle images can leave the image during the interval time and are therefore not used in the evaluation step. It is advised to have at least 5 particle images pairs in the interrogation windows to get accurate results (RAFFEL, WILLER, WERELEY, & KOMPENHANS, 2007). This can be adjusted directly on the smoke machine or changing the size of interrogation windows. However the second method can induce errors and a loss of resolution as will be explained later. When using the recording menu of Davis and thanks to the panel on the left and selecting areas of interest, it is possible to get immediately values from a recorded image like particle image sizes and intensities (LAVISION GmbH, 2010). However these values are strongly dependant on the quality of the images and can only be considered as an help.

Particles light intensity

As explained earlier, position of cameras in the case of S-PIV gives better results if it is forward from the laser sheet direction than backward. This is due to the way particles reflect the light from the laser. Reflection of the light around the particles corresponds to the Mie´s scattering theory describing the electromagnetic radiation by a sphere. In Figure 15 is represented the Mie´s scattering of oil droplets around 1μm of diameter in air and using a 532nm laser. Other Mie´s scatterings for other diameters, particle materials and surrounding flows are visible in (LAVISION GmbH, 2011) and (PRASAD, 2000).

Sometimes it is not possible to arrange camera positions as whished. They can be both in the backward direction, like for this project, or one backward and one forward. In this cases, it is important to play with the aperture of cameras in order to capture the same light intensity with all cameras. Decreasing the aperture or increasing the f# of cameras, the light intensity is also decreased. Although that should be done carefully because it will also increase the particle images size as explained earlier.

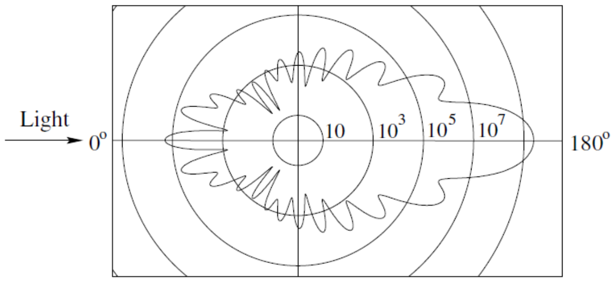

Figure 15. Scattering of the light around oil droplets of 1μm of diameter. Logarithmic scales are used to describe the intensity of light reflected by the particle depending on the angle of view of the camera.

During PIV image recording, the particles are illuminated by the laser sheet and the important parameter is actually the signal-to noise ratio meaning the contrast between light intensity reflected by particles and the light reflected by surroundings. This signal-to-noise can be improved by increasing the power of the laser and so the light reflected by the particles but the noise in the background needs to stay of the same order; if both are increased, the ratio remains the same; the results will not be improved but the camera sensors could be destroyed. A meticulous study of reflections coming from surroundings is thus needed.

An important thing to remember with CCD cameras is that they are extremely sensible to the light intensity and their sensors can be destroyed if it surpasses a limit; in order to avoid this, the laser always need to be used carefully and its power increased little by little controlling the intensity on the images to be sure that it remains under the limit everywhere in the field of view. Using DaVis software, in the recording panel, it can be chosen to see ‘statistical’ properties of the images next to them, the minimum and maximum of light intensity recorded by the cameras for the image can be controlled there and should not reach the limit of 10000 counts.

2.2.6. Techniques used to reduce laser reflections

The main problem that occurred when running PIV measurement for this project was the reflections of light. They were caused by reflections of the laser beam both on the front and the back of the glass-cylinder and on surrounding objects. The ones on the cylinder wall are represented in red in Figure 16. Their intensities were strong enough to destroy the camera sensors if laser power were turned up from minimum so they couldn’t just be removed during the pre-processing step (explained later). One needed a method to get rid of them before taking the pictures.

The method used for most of the measurements during the project didn’t remove the reflections but caught them behind an opaque surface. Black adhesive tape has been placed on the cylinder surface in front of both cameras to intercept reflections paths. This method is really efficient since no reflections are left and a high laser power giving really good view of the particles can be used. However, it presents some difficulties to be used. First, paths of the laser reflections (red dashed arrows in Figure 16) are actually not visible by the human eye without risk of injury so the only information to find the intersection with the glass cylinder (black dots) are the recorded images using the laser at low-power. This makes it difficult to find the exact location and a larger surface than the one actually needed is generally covered. The consequences are a reduced field of view, about 25% of the bore of the cylinder was hidden by this tape. Other techniques have therefore been tested.

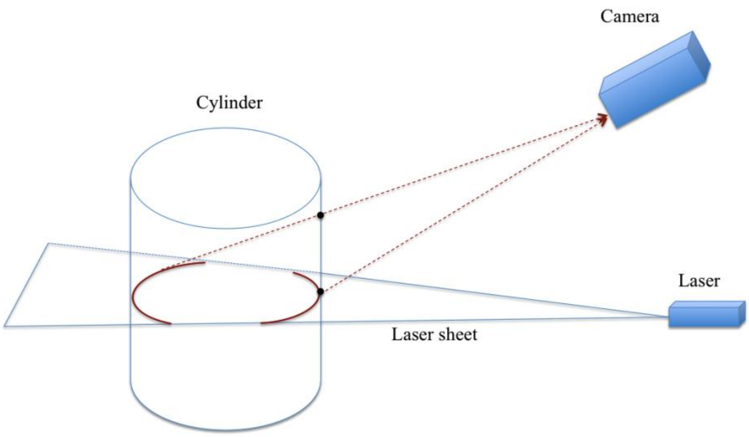

Figure 16. Reflections of the laser on the glass cylinder wall. Two different kinds of reflections in red; ones produced by the laser beam entering in the cylinder and on the back of the cylinder. Dashed arrows represent their paths from the reflections sources to the cameras lenses. The black dots are the intersection of these paths with the forward surface of the cylinder.

The fluorescence principle

The white light is composed by overlapping of all the color of the rainbow. Each color is an electromagnetic radiation with a certain wavelength and frequency. The laser used with PIV is green and composed by only one wavelength; 532nm.

Fluorescence is an interesting phenomenon; fluorescent objects are able to shift some wavelengths coming toward them and so reflect a different wavelength than the source. This means that they can be lighted up only with the green wavelength of the laser and seen of a different color like orange. The fluorescence ‘shift’ is only possible from a low wavelength to a higher wavelength; e.g. an object lighted up by an orange light can’t be seen green. The principle of fluorescence is described in Figure 17.

Fluorescent particles are often used when running PIV measurements of liquid flows (LINDQUIST, 2005), (GURLEK & SAHIN, 2010), this is even indispensable when running micro-PIV (OISHI, KINOSHITA, FUJII, & OSHIMA, 2011). Instead to reflect a light with the same wavelength as the laser, they reflect a orange light. A high-pass filter (Figure 17) for which only wavelengths above the threshold can go through is put in place on the lenses of the cameras in order to keep only the orange light. Green reflections of the laser on droplets in the liquid or on surfaces are therefore not seen by the cameras. Due to its high efficiency to remove reflections of the surrounding, this principle was tried in this project.

This process is possible because the liquid is in general contained in a closed-circuit. For this project, fluorescent particles couldn’t be used since the air flow is released in the atmosphere after running so the reverse was tried. Instead to use fluorescent particles, some parts of the cylinder’s wall and surrounding objects were painted with an orange fluorescent paint in order to transform all reflections that could destroy the cameras sensors to orange. The fluorescent paint used has been chosen to be the same as the one used in (LINDQUIST, 2005) because the author showed that it has good fluorescence properties and even did a fine study of the wavelength reflected by the paint. Then, instead of using high-pass filters, band-pass filters 10nm large with a central wavelength of 532.5nm were applied on the cameras in order to let only the green reflected by the particles going through.

First tests have been made using white paper and applying fluorescent paint in some places. These tests gave promising results (Figure 18), almost no light was reflected on the painted parts. However, other tests showed that this technique is only efficient when using it on mat surfaces. Since the conversion rate of the wavelength of the fluorescent paint is not 100% efficient and filters can't filter perfectly (there is always some other wavelengths going through), the reflections over the paint is still a bit higher than the one of the laser directly on the transparent glass cylinder. This technique can therefore only be used to avoid reflections from surrounding objects but not from the cylinder wall. However the filters remove some of the noise during the recording and make the calibration easier.

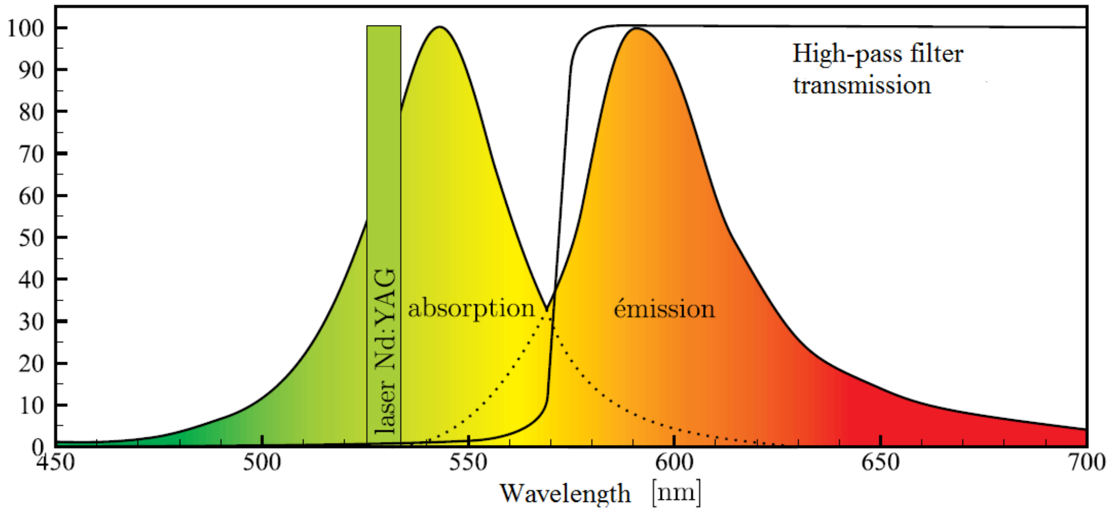

Figure 17. Principle of the fluorescence. The fluorescent object shifts wavelengths of the curve **'absorption' in the ones called 'emission'; it will be seen orange even if it is only lighted up by the** Nd:YAG laser. A high-pass filter is also represented. (LINDQUIST, 2005)

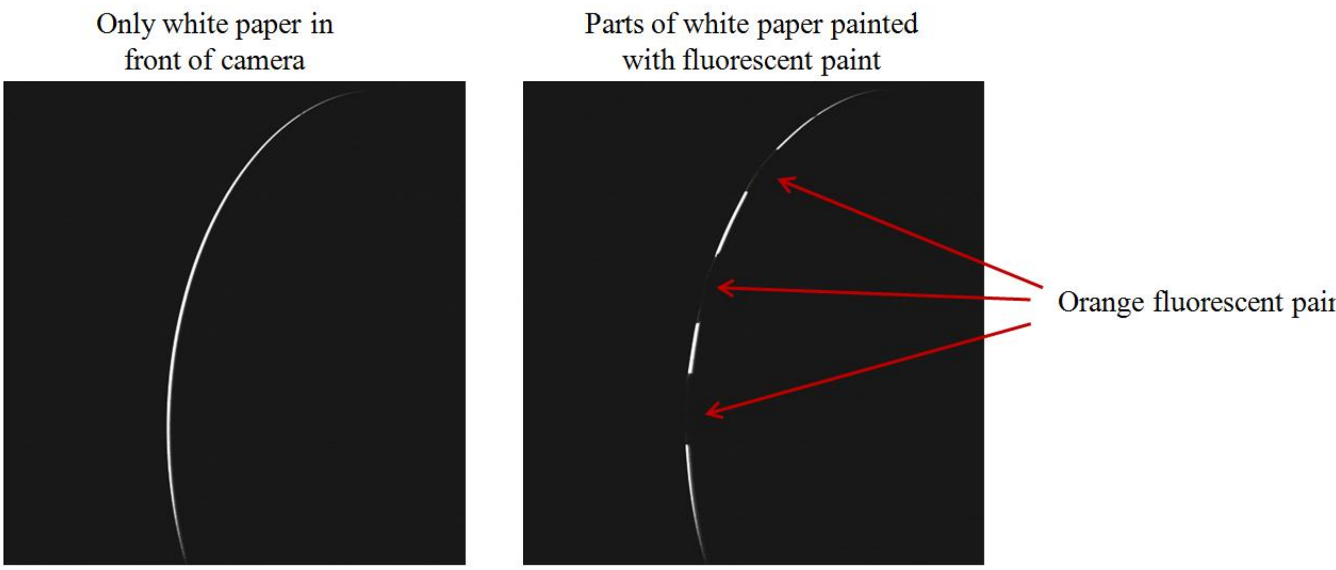

Figure 18. Tests of the orange fluorescent paint on white paper using a band-pass filter on the camera.

2.2.3. Calibration

In order to convert camera pixels to the physical length scale, [m], calibration is needed.

With PIV and a camera perpendicular to the laser sheet and taking direct pictures of the flow, only a scaling step is necessary in order to achieve pixels dimensions. The user uses the menu 'scaling' in Davis, taking an image and selecting two positions on it with a known distance. Giving this information to Davis, the algorithm is then able to do the conversion pixels to meters that is needed.

When the view of the cameras is not at 90 degrees and/or if the images are distorted, conversion responds to a more complex algorithm than just a scaling, a complete calibration is then compulsory. S-PIV measurements always need this step since the cameras are not perpendicular to the laser sheet. Moreover this step makes it also possible to couple the images from the cameras. To do the S-PIV reconstruction for the PIV evaluation of each camera, the algorithm needs to know where a physical position (x_0, y_0) is represented on the images of camera 1 (x_1, y_1) and camera 2 (x_2, y_2). Finally, the calibration will also correct distortions of the images due to the recording through the glass cylinder.

The calibration for S-PIV measurement is therefore more complex than the scaling for PIV and can induce errors in the PIV results whereas a wrong scaling step induces only errors in the conversion of the PIV results.

S-PIV calibration principle and mapping function

The calibration for S-PIV is made using a 3D calibration plate with marks on two levels to be able to calibrate the three dimensions of space (Figure 19). Obviously the calibration plate has to be placed at the same place as the laser sheet or at least as close as possible. Although it is sometimes not feasible and so techniques have been developed to solve this problem (Cf. later), (WIENEKEN, 2005).

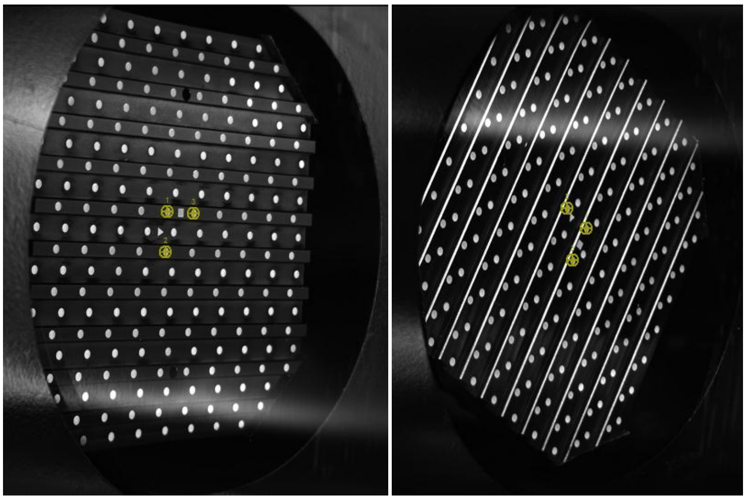

Figure 19. Pictures of the calibration plate with camera 1 (left) and camera 2 (right). Yellow marks used to correlate the cameras are visible is the center of the plate.

When starting the calibration step, a coordinate system is chosen (in this case a left handed one with z-axis turned downward), the type of plate used is chosen, the focus for each camera is done and three identical marks for all cameras are pointed on the images. These marks have to correspond on the same physical dots on the calibration plate for all cameras in order to get a correct correlation. The software is then able to identify the white dots on the calibration plate thanks to the difference of light intensity. Positions of these dots are used to evaluate coefficients of mapping functions which are applied to correct the distortions due to the glass cylinder, determine angles of view (α_1 and α_2 in Figure 11) and fit together images coming from the two cameras; it converts the 2D recorded planes into the 3D physical plane. With S-PIV measurements, two mapping functions need to be determined (one for each camera) in order to transform the pixels localizations (s_1, t_1) for images from camera 1 and (s_2, t_2) for images from camera 2 into the (x, y) coordinate system and then (x, y, z) with the S-PIV reconstruction. Different mapping functions can be used with DaVis software; the pinhole model or the third order polynomial. For this project the pinhole is not recommended since the images are taken through a glass cylinder and are therefore subjected to strong distortions (WIENEKEN, 2005), the appropriate model is the third order polynomial which is (FEI & MERZKIRCH, 2004):

$$\begin{cases} x = a_1 + a_2 s + a_3 t + a_4 st + a_5 s^2 + a_6 t^2 + a_7 st^2 + a_8 s^2 t + a_9 s^3 + a_{10} t^3 \\ y = b_1 + b_2 s + b_3 t + b_4 st + b_5 s^2 + b_6 t^2 + b_7 st^2 + b_8 s^2 t + b_9 s^3 + b_{10} t^3 \end{cases}$$

x and y are the global coordinates while s and t are the coordinates in the recorded planes. This is the mapping function for only one camera. When using the third order polynomial mapping function, it is recommended by LaVision to use a calibration plate large enough to cover all the area of interest. The algorithm calculates the coefficients of the mapping functions using the white dots and their global coordinates already known by the software. It tries to fit a maximum of points but it is never perfect even in cases with no distortions, so the deviation between the global coordinates of dots and the one given by the mapping functions is evaluated for each mark and averaged over all the plate. The mapping function giving the smallest deviation is then chosen by the software. The remaining averaged deviation is the so called RMS of the function and should be less than 0.3. However, dealing with strong distortions, in general, a so small value cannot be reached but can be corrected with the self-calibration step.

Once the calibration step is finished, the laser sheet can be put in place using the calibration plate to be sure that it is in the focused area and horizontal. The cameras need to be protected during this step because even if they are off, reflections of the laser sheet on an object can destroy their sensors. Although, the laser sheet will never fit perfectly the position of the calibration plate and so the focus of the camera needs in general to be adjusted when using the particles and a step of self-calibration must be executed with few recorded images. More details about how to realize a correct calibration step are given in (LAVISION GmbH, 2011).

Self-calibration

Since the adjustment of the laser sheet position is done manually on the calibration plate, they cannot be perfectly aligned; there will be a remaining angle or translation between them that can induce errors during the processing step. Indeed when the laser sheet does not coincide with the calibration plane used to determine the mapping functions, one particle can be seen at different positions by the cameras and so be interpreted as two different particles. So stereoscopic PIV measurements need a step of 'self-calibration' in order to line up the calibration plane and the laser sheet.

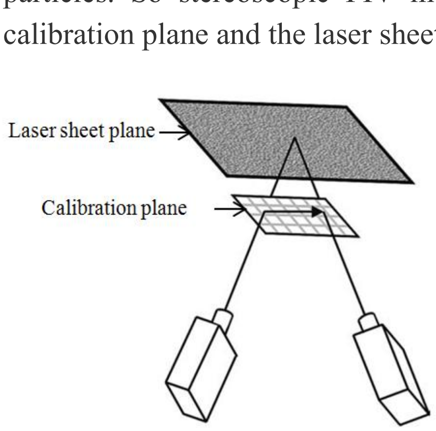

Figure 20. Representation of one disparity vector, the cameras look at the same particle in the laser sheet plane which is not aligned with the calibration plane. The particle is therefore seen as two different particles separated by the disparity vector in the calibration plane (WIENEKEN, 2005).

To realize this step, between 20 and 100 images should have been recorded and a size of interrogation windows chosen (usually it can be 64×64 pixels). An option doing several passes (as when doing PIV evaluation as explained later) can be chosen. However it takes longer time and doesn't give better results. The software will then compute the disparity vectors linking two representations of the same particle in the plane of the calibration plate (Figure 20). Using a triangulation methods, DaVis is then able to determinate the global coordinates of the particle in the laser sheet plane and therefore adjust the mapping functions to this plane and decrease its RMS value (from 1.2 to 0.04 for example in one of the studied cases).

Once the step of self-calibration is finished, the user has the choice to accept the new calibration parameters or not and to re-calibrate the images already recorded or not. One needs in general to repeat the step several times (between 2 and 4 times is in general enough) to give satisfactory results. The user should chose to accept the new parameters each time but wait till the end of the last step to re-calibrate the images because it can be time consuming.

2.2.4. Time delay between frames

As it has been explained earlier, the most current method to take the pictures consist in taking one frame of each laser pulse with each camera in order to proceed to a cross-correlation and be able to determine the direction of the movement . The two laser pulses and recording times of the cameras have to separated by the same time delay called Δt.

This Δt is dependent on the velocity range of the flow in the area of interest. If the time delay between the two frames is too small, compared to the velocities, the displacement of some particles during this time could be less than one pixel. In these cases, the determination of the exact value of displacement and the velocity of these particles will only be determined by the sub-pixel estimator. A peak-locking error as small as possible is therefore necessary to get accurate results. On the other hand, a too long time delay also gives errors in determination of both out-of-plane and in-plane velocities. If too many particles went out of the laser sheet between the recording of the two frames, due to the out-of-plane velocity, too much information is lost and the maximum velocity in this direction will be determined to be inferior to the exact one. Particles that would eventually remain in the laser sheet could cover a too long distance during the interval time and the algorithm will need large interrogation windows to do the correlation; the resolution of the results will be decreased. In some particular cases for which the velocities are too widely spread, it is not even possible to find a time delay which makes possible to catch the lowest and the highest velocities of the flow and different studies with different Δt is need to be made to study all of the flow area.

To avoid problems due to the out-of-plane velocity, displacements perpendicular to the laser sheet occurring between the two laser pulses should remain inferior to one quarter of the laser sheet thickness (KIGER). Since the velocity parallel to the axis of the cylinder is known to be higher than the ones in the observation plane in the case of the intake stroke, this law can give an order of idea of the time interval that should be used. The characteristic velocity in the case of the in-cylinder flows of internal combustion engine is known as (HEYWOOD, 1988):

$$v_0 = \sqrt{\frac{2\Delta p}{\rho}}$$

The time delay have been tested with a pressure drop of 981 Pa across the test section:

$$v_0 = \sqrt{\frac{2 \times 981}{1.2}} \sim 41\, m/s$$

Recall that the laser sheet thickness was about 2 mm:

$$\text{displacement during dt } < {}^{1}/_{4}\,\Delta z \quad \rightarrow \quad \text{dt } < 12\,\mu s$$

This characteristic velocity corresponds to a maximum value that the flow could reach somewhere in the cylinder, in general close to the valves. As it will be seen later, the maximum velocity parallel to the axis of the cylinder in the plane used for this study is much smaller so the interval time can be increased. Anyway this law is interesting because it gives a first approximation of Δt.

Another method to determine the optimal time delay is to look at the pixel-displacement of the particles between the frames. Starting with a really small time delay like 1µs, Δt is increased step by step until the displacement of particles reaches 5 pixels; the last one correspond to the optimal one for the measurements. That can be done directly by the user taking one picture of two frames for each dt and processing it directly in the recording dialog of the software. Holding the 'shift' key and sweeping the vectors result with the curser, the displacement of the windows of interrogation can be read in the right and low corner of the software window. In recent versions of Davis an option called 'dt optimizer' appeared. This option uses exactly this iterative method to find the best time delay taking into account a maximum particles displacement of 5 pixels and controlling at the same time that the correlation values are still correct. This option needs some adjustments; the user needs to select an area of interest where the flow occurs. Actually, the option doesn't work if the algorithm tries to determine a dt for all the image whereas some parts of it are not flow, but it should be kept in mind that this area should cover all range of velocities; if the highest velocities are not in the area, the dt given by the 'dt optimizer' will not be small enough and the other way around. To use the option, only one camera must be working at a time and taking two frames. The 'dt optimizer' option indicated that the interval time should be between 16 and 20µs.

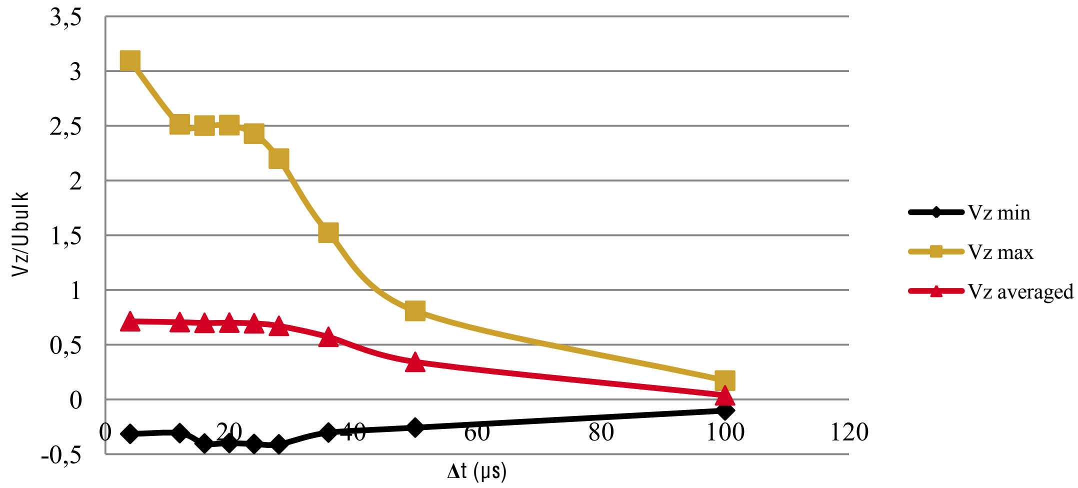

Figure 21. Evolution of the mean out-of-plane velocity in function of the time interval applied between the frames.

Different time delays have been tested in order to show rapidly the efficiency of the 'dt optimizer'. The same experiment has been run with time intervals from 4 to 100µs. It can be seen in Figure 21 that, when the time interval increases, the maximum out-of plane velocity catching by the PIV decreases, the particles having higher velocities went out from the laser sheet and so are not considered. It can also be observed that the results for times delays equal to 16 and 20µs are really similar. The differences in the mean velocity between the two cases is inferior to 0,1 m/s which is perfectly acceptable with PIV measurements. The results for Δt equal to only 4µs seems to give an even higher result for the third coordinate of the velocity. However, the complete pdf of the instantaneous velocities shows that the range of displacements of particles during the interval time is too small when Δt is only equal to 4µs; only 2 pixels in each direction for x-displacements instead of about 3 pixels with 20µs (Figure 22). The results are therefore not accurate because of an important lack of precision.

The 'dt-optimizer' seems to be a correct and fast method to determinate the accurate interval time and was therefore used for other measurements of this project.

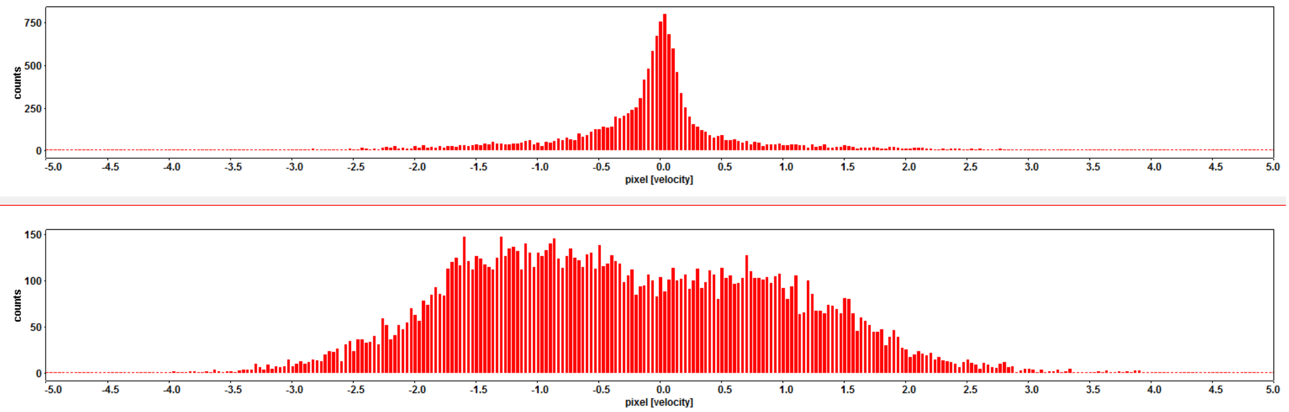

Figure 22. Probability Density Function of one instantaneous velocity field along the x-axis for Δt equal to 4µs (higher one) and Δt equal to 20µs (lower one).

2.2.5. Number of pictures

As explained earlier, each picture or set of 4 frames handles the instantaneous velocity field of the flow so the number of pictures that need to be acquired is only dependant of the studied flow. Indeed, most of the observed flow with PIV are turbulent flows and therefore an average on time or sample needs to be executed to get a mean flow field.

For example, in this project a large number of pictures has been taken, in general between 1000 and 1500 images and the mean velocity field has been calculated with all of them but the results showed that an average over a sample of about 750 images would have been enough.

2.3. Processing and evaluation of the results

Once images with good quality have been recorded, one can start the S-PIV evaluation. The software DaVis contains a lot of different options to realize it. The usual method to get the most accurate results is to apply successively.

- a pre-processing to increase the quality of the recorded images,
- the process or evaluation can also be realized in different ways, choosing the windows of interrogation and their size as well as the number of evaluations with the multi-pass option,
- finally a post-processing over the velocity vectors in order to remove all the spurious ones.

This method is used to get the instantaneous velocity components. However it is sometimes helpful to start the process applying only the simplest PIV evaluation to the recorded pictures in order to judge their quality; one can send the pictures and/or the velocity field evaluated to the 'Correlation Map'. One may use the three dimensional view for better understanding and interrogation windows of the same size as the one used for the evaluation. Figure 23 shows two different correlation maps giving extreme information. On the left, it can be observed different peaks with the same height and no one higher than the others. The dominant peak on the picture on the right corresponds to the maximum of the correlation function as earlier explained. It has to be clearly identifiable among the others to validate the resulting velocity vector.

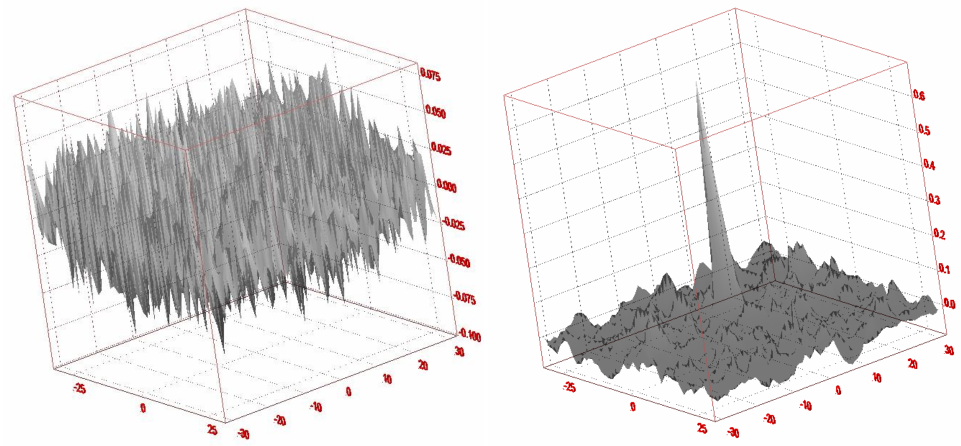

Figure 23. Example of two three dimensional correlation map using interrogation windows of 64×64 pixels. On the left, the correlation function cannot find an optimal pixel shift whereas on the right it handles a dominant peak corresponding to the maximum of the correlation function.

2.3.1. Improvement of the pictures quality through the pre-processing

Masking function

The first step of the pre-processing of the images is to apply a mask on the parts that are not interesting for the study. The algorithm will not work on these areas when processing and therefore time will be saved and errors reduced. Even the step of self-calibration gave better results when working on the masked images than with the whole picture.

There are different methods to mask the images available in DaVis. The simplest way is to draw a 'geometric mask' but it works only when the limit of the area of interest is steady because this exact mask will be applied to all the images. For this study, the observed horizontal plane where the flow occurs is only limited by solid and immobile surfaces like the cylinder glass or some pieces of tape. The geometric mask could therefore be used. When the limit between the studied flow and surroundings is moving depending of the flow the 'algorithmic mask' can be used instead. In this menu, one can chose different options to create a mask that will adapt for each image. For example, the user can chose to mask the pixels for which the intensity is below a certain value because they correspond to pixels outside from the flow field. In the other way around, it can be chosen to mask pixels with a light intensity higher than the one produced by the particles. These options need to be used carefully because pixels useful for the PIV evaluation can be masked and so generate a lack of information and errors. More information about the 'algorithmic mask' is in the manual (LAVISION GmbH, 2011).

Improvement of the signal-to-noise ratio

The parameter of paramount importance when using PIV evaluation is the ration between the light intensity from the particles and the one coming from the surrounding; the signal-to-noise ratio. Different methods can also be used to, first, reduce the noise and even improve the ratio.

The first method consists in separating the two types of noises present in the pictures. The first one is the noise due to the camera. It is the one visible when recording an image with the caps on, called a dark image. The resulting picture is not totally black; the light intensity is of order of 100 counts and not zero, as it would be. The second type of noise is due to the background of the observed area. This method needs to be prepared before recording the pictures since a dark image (with the caps on the cameras) and an image of the background (in exactly the same conditions as the recording will be, same laser power, same area but without the particles) needs to be recorded too. Then the light intensity captured by each pixels on these two images will be subtracted to the one of the recordings with the particles (HONKANEN & NOBACH, 2005). One can chose to subtract it directly during the recording of the data and therefore get already corrected images but in order to keep a maximum of information it is better to subtract it oneself once the image have already been recorded. In Figure 24, the process of correction is described, the picture on the left is a recorded image without any correction except the application of a geometric mask and the plot below is the light intensity along the red horizontal line. Then subtracting the dark image from it, the noise from the camera is corrected; it can be read on the intensity plot that at the extremities, where there is no particles, the intensity is now equal to zero. The last step is the correction of the background reflections. The most visible one is the reflection on the left of the red line, between the limit of the mask and the particles, on the intensity plot; this reflection induced a strong peak that has been removed on the plot on the right.

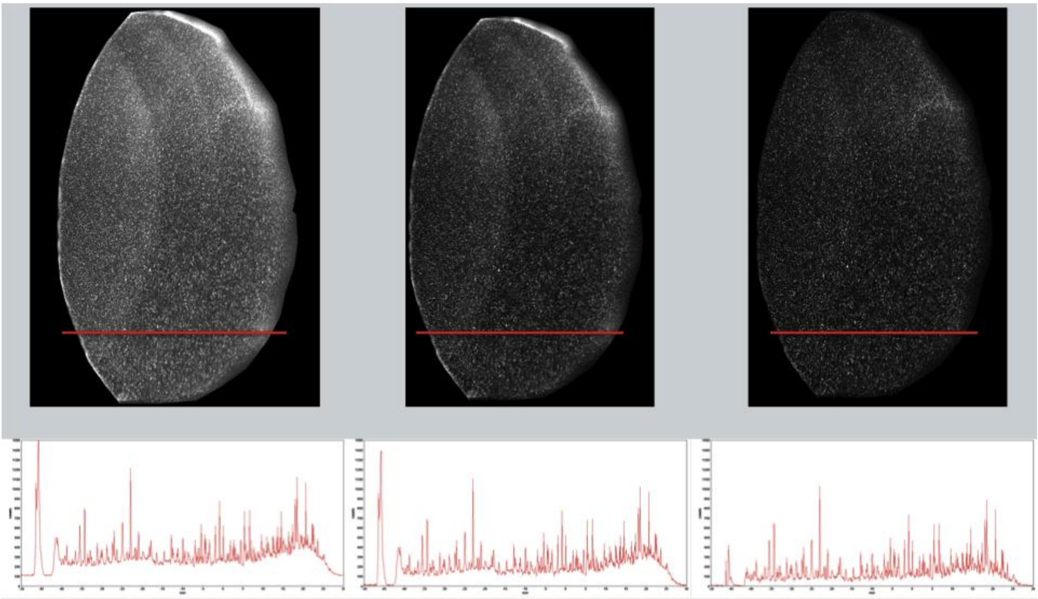

Figure 24. Correction of the noise due to cameras and reflections from backgrounds. The repartition of the light intensity on the red light is plotted below the recorded picture. The image on the left has not been corrected yet, in the middle the dark image has been subtract and finally on the right one the background is removed.

This method gives visible improvement but other processes that can be used with Davis are actually more efficient because they work both on the correction of noise and reflections but also improve the particle image sizes and their distinction with the background; all the aspects of the signal-to-noise ratio.

This process can be executed either in the menu pre-processing of the PIV evaluation called ‘vectors calculation: doubles frames’ or using the menu of pre-processing of the ’time-series PIV’.

The first option using the pre-processing panel of the S-PIV evaluation is executed in three steps (Figure 25);

- 'Subtract sliding background' is the first step. The algorithm is calculating the sliding minimum of intensity over a number of pixels. This quantity needs to be defined by the user and should be equal to 4 or 5 times the particle image size. Then this minimum is subtracted to the image.
- The second step corresponds to the particle intensity normalization: A length scale needs also to be set here and should be this time equal to more or less the particle images size. Two maxima are computed; a local and a global. The local correspond to the maxima over a windows with a size of the length scale. The global maximum is computed over a window with a size of ten times the length scale. Then the ratio between the global and the local maxima is calculated.
- Finally the results from the two first steps are multiplied.

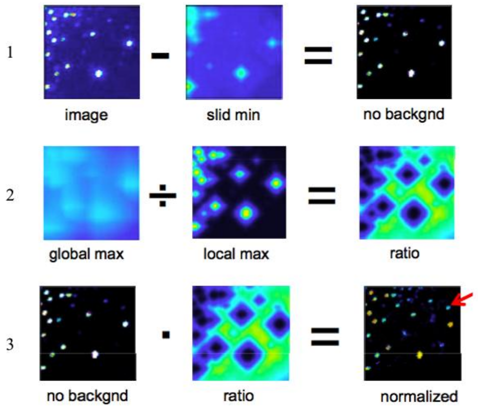

Figure 25. The three step of the signal-to-noise correction using the pre-processing of the S-PIV dialog, the first step correspond to the subtract of a sliding background and the steps 2 and 3 are the ones of the particle intensity normalization (LAVISION GmbH, 2011).

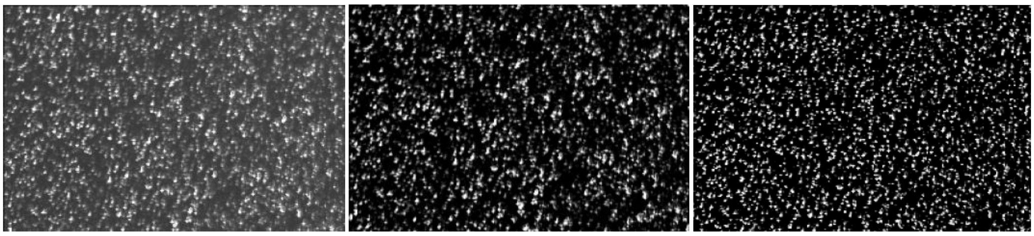

Figure 26. Evolution of the particle images **when applying the 'subtract sliding background' between** the first and second **images and then the 'particle intensity** normalization before the third image.

The second option, 'time-series PIV: subtract absolute min over time' is scanning all the images of the set one after the other in order to find the minimum of intensity of each pixel through the set. This is the main difference with the previous option; it was applied at each pictures whereas this one is working on all the set of pictures together. The result is therefore an image created thanks to all these minimums and is then subtract to each image of the set. This method is giving good results in most of the cases and has been the one used when using S.PIV evaluation on GPU. Although this could not be perfect if the reflections are not stable and move during the recording, since this option is looking for the minimum of intensity, it could miss them and not remove them.

2.3.2. The multi-pass option of the S-PIV evaluation

Once the pictures have the best signal to noise ratio, the evaluation of the vector field can start. The process explained in the introduction of this chapter is the principle of PIV evaluation and has been strongly improved these fifteen last years. Nowadays, several evaluations with varying interrogation windows size can be applied successively. A pre-shift of their position, also called window deformation, improving the determination of the pixel displacements can be used as well as other interesting options that will be explained here.

As previously explained, the interrogation window size is a determining factor for the quality of the results. Each couple of interrogation windows handle one instantaneous velocity vector. A subdivision of the images using large windows will therefore decrease the resolution of the results. Moreover, the particles contained in the same window must have a homogeneous movement since the correlation is working on the intensity shift; if all the particles move in different directions with different velocities, the grey distribution shape will be lost during the interval time. This notion is important dealing with turbulent flows especially in the center of vortices where the velocity direction can be really different and so the interrogation windows size can't be chosen too large. However, a number of 5 particle images pairs are necessary to get a correct correlation value during the evaluation. Depending on the velocity of the fluid and so of the particles, an important loss of particle images can happen during the interval time separating the two frames. The size of the interrogation windows can therefore not be too small either.

A first solution using large interrogation windows is to add an overlapping between them (25, 50 or 75%). The size will remain unchanged but the number of interrogation windows and so the spatial resolution will increase. However, the problem of evaluating flows with inhomogeneous movements is not solved, motions with scales inferior to the window size will not be taken into account. The best way to improve resolution and accuracy of the results if therefore to apply a 'multi-pass evaluation' for which the efficiency has been proved in (STANISLAS, OKAMOTO, & KÄHLER, 2003).

Its principle is to execute successively several evaluations starting with large windows size and switching to smaller ones. The first evaluation handles an accurate but coarse vector field. Then the algorithm is able to evaluate the displacements with smaller windows using a 'window deformation'. It takes into account the previous results before to apply the algorithm of cross-correlation. Let's say that the first pass handled a pixel displacement of (dx, dy) between a couple of interrogation windows. Before to run a second time the evaluation, the algorithm will shift the first frame window of (-dx/2, -dy/2) and the second frame window of (dx/2, dy/2) from their initial positions (Figure 27). In Figure 27, the interrogation windows size is kept constant but the user usually chose to decrease it since problem due to a too high loss of particle image couples is avoided using the window deformation, the resolution of the results is therefore increased. Figure 28 represents the steps of the multi-pass evaluation. Several of these steps are actually validation steps.

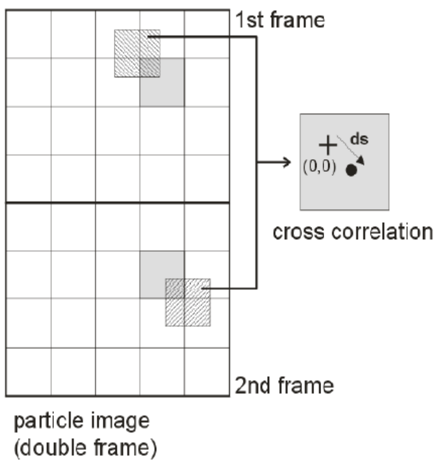

Figure 27. **Example of the 'window deformation', windows of each frame are moved of half the** displacement handled by the previous evaluation step (ds). In this case the size of the interrogation windows is kept constant.

Different shapes of interrogation windows can also be used. The circular ones gives better results than the squared ones specially in regions near to borders but the process is more time consuming. To get more information about these window weighting function, see (LAVISION GmbH, 2011) and (LAVISION GmbH, 2010). When running S-PIV, this method is obviously applied to the recorded images from both cameras, Once the results for PIV evaluation for each camera are validated (see next part), the S-PIV reconstruction is applied.

For this project, the multi-pass evaluation with decreasing windows size has been used. The first evaluation step was made with interrogation windows of 64×64 pixels and 50% of overlapping. Then 2 evaluation steps were applied to circular windows of 32×32 pixels and overlapping of 75% which gives a distance of 632 µm between each evaluated vector.

2.3.4. Vector validation

Once the evaluation of the velocity vectors has been done, methods to validate them are applied in order to reduce errors. This step of validation is applied to the final vector field but also between each pass of the multi-pass S-PIV evaluation as Figure 28 shows. Different filters can be used with DaVis to get rid of potential 'spurious vectors'.

The different options that are available are well explained in (LAVISION GmbH, 2010) and summarized here:

- If the flow behavior is already known, a range for the velocities can be used. All the velocity vectors outside from this range will be deleted.
- A filter working on the correlation value can also be used. One can chose to delete vectors with a too small correlation value or look at the ratio between the highest peak and the second peak.
- The median filter works with a mean value calculated over neighboring vectors. The RMS between this mean and neighboring velocity vectors is calculated as well as the deviation between the considered vector and the mean. A threshold is defined by the user to either delete the vector or replace it using the second or the third highest correlation peak.

Other functions are available to interpolate or smooth the final velocity vector field like smoothing function but the user should be careful using to strong post-processing not to lose information and finally induce errors.

During this project, PIV evaluation using only the CPU of the computer and PIV with the GPU have been run using the multi-pass option. This option include automatically a post-processing step that the user can't cancel. The algorithm for the PIV on CPU and the one on GPU being slightly different, their results showed some differences. The results of the evaluation on the CPU showed few spurious vectors in some instantaneous velocity fields. A post-processing step has therefore been applied on the velocity fields resulting from the evaluation with the CPU. The vector evaluation deleted all vectors with a correlation value inferior to 0.6, used a median filter to remove the ones for which the deviation to the mean value calculated over neighboring vector is 1.5 times higher than the RMS of the neighboring values with this mean. After this last step, differences between resulting velocity field from both PIV on CPU and PIV on GPU were not visible anymore.

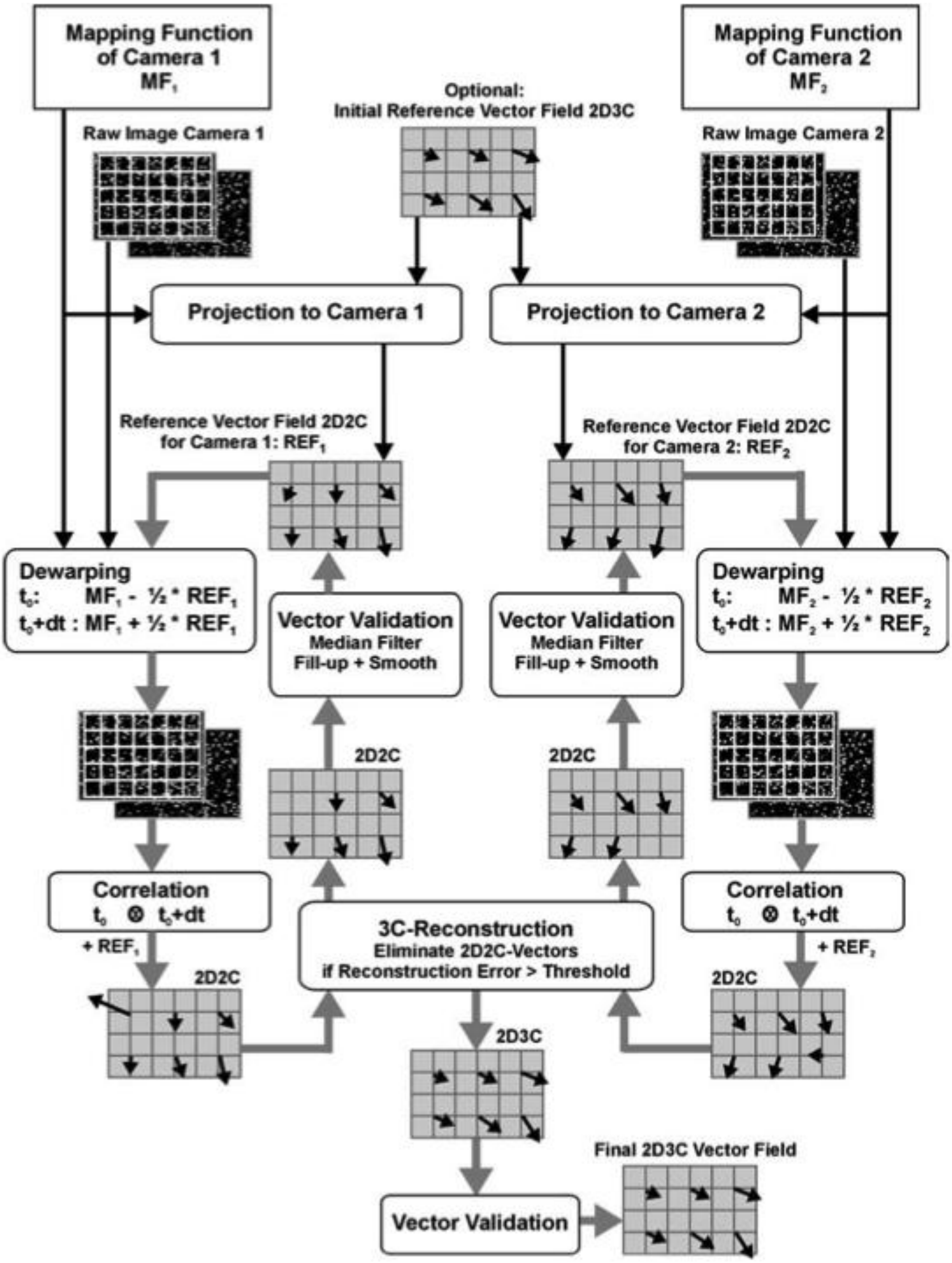

Figure 28. Description of the multi-pass S-PIV evaluation process. On the left, the images from camera 1 are analyzed; the ones of camera 2 are on the right. The results from previous evaluations are used to realize the next step and vector validations are applied in order to remove some spurious vectors. Here squared interrogation windows with 0% overlap are represented.

Chapter 3: Intake in-cylinder flows; results and discussion

3.1. Introduction

The cylinder head with ports and valves used for testing was a model usually produced for the six cylinders inline Scania engine.

Positions of the inlet valves 1 and 2 can be observed in Figure 29. The coordinate system used to present the results is also shown in Figure 29. A left-handed coordinate system has been used in order to represent the component of the velocity parallel to the cylinder axis which is positive when the flow is going from the head cylinder to the flow bench.

The horizontal plane studied is 165mm below the valves (Figure 29) which is only few centimeters above the plane where the honeycomb was placed to measure the swirl ratio in the steady flow bench.

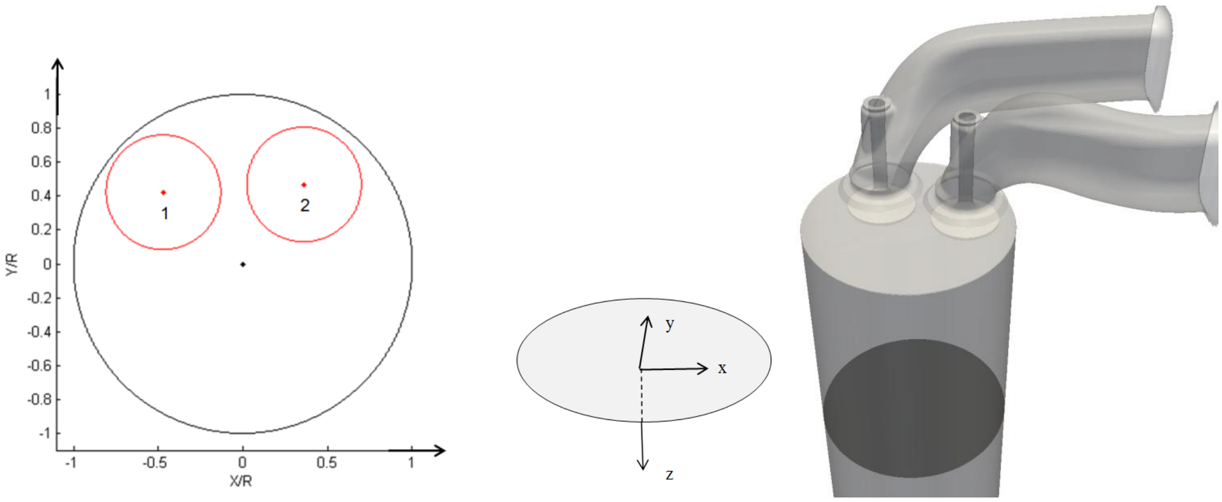

Figure 29. To the left, the projection of the inlet valves (red circles) is represented on the area of interest (when looking from above the cylinder), the port and valve designs as well as the area of interest (dark surface) are visible to the right. The figure in the middle represents the left-handed coordinate system used to present the results.

3.1.1. Plan of experiments

Different cases with different inlet parameters have been studied during this project. As explained in the first chapter, many in-cylinder flow measurements have been performed in non-steady conditions, working with a piston and for different crank angles in previous studies. The study here has been performed without piston and at steady mean flow and valve lift utilizing the flow bench used for honeycomb measurements. Different inlet valve openings have been used; the valve lift can later be mapped to the crank angle for computing the mean swirl ratio (Figure 4). When the valve lift is equal to 5mm, the valves are almost closed and when it is equal to 15mm, the opening is close to its maximum. Different pressure drop measured between the atmospheric pressure in the room and the pressure at the end of the flow bench have also been used for each valve lift. This parameter is a function of the speed of the engine, since higher engine speeds give higher piston velocity and thus a higher pressure drop.

The table of experiment (Table 1) summarizes all the parameters tested and names the different cases. Constant values used during experiments can be found in Table 2.

Case	Number open valve	Valve lift [mm]	Δp [mmH2O]	Δp [Pa]	Air density [kg/m^3]
A_1	2	5	80	784	1.195
A_2	2	5	140	1372	1.193
A_3	2	5	245	2402	1.188
B_1	2	11	80	784	1.195
B_2	2	11	140	1372	1.193
B_3	2	11	245	2402	1.188
C_1	2	15	80	784	1.195
C_2	2	15	140	1372	1.193
C_3	2	15	245	2402	1.188
D_1	1	11	80	784	1.195
D_2	1	15	80	784	1.195

Table 1. Experimental parameters for PIV measurements

Room temperature	Atmospheric pressure	Distance between measurement plane and cylinder head	Cylinder diameter	Piston stroke
274 K	1.013×10^5 Pa	165 mm	130 mm	154 mm

Table 2.Constant parameters for PIV measurements and results evaluation

The air density has been evaluated for each case as the average of the density calculated by the atmospheric pressure (p_{atm}) and the density evaluated with a pressure equal to p_{atm}-Δp, which means that the air density is slightly different between all cases. The flow can be seen as incompressible in the area of interest since the Mach number is less than 0.3.

Knowing the pressure drop, the type of valves, the valve lift and the density of the air, the exact volume flow across the valves has been measured for each case tested using the honeycomb measurement procedure (LINDGREN, 2003). From this volume flow and the diameter of the cylinder, the bulk velocity corresponding to each case has been determined and used to normalize most of the results. Various positions like the position of the area of interest will be normalized by the diameter of the cylinder. The weighted averaged swirl ratio evaluated for the cylinder head using the honeycomb measurements has also been used to normalize the swirl ratios (SR) resulting here. These SR have been evaluated using the formula described in the chapter about internal combustion engines (eq. (5) and (6)).

As can be seen in Table 1, some experiments have been run with only one valve open. The valve kept open is number 1 in Figure 29.

Since the recordings have been made with constant pressure drop, valve lift and thus steady mean flow, an ensemble average has been used to get the mean field of each case (eq. (1)). More than 1000 instantaneous velocity fields was measured for each case. Most of the studies have been made over all the available data even if the results showed that neither the estimation of the mean nor the studies of the fluctuations needed more than 750 instantaneous velocity fields.

3.1.2. Field of view

It was not possible to determine the position of the center of the cylinder by simply looking at the images. But in some images of the particles taken with both the camera 1 and 2, the cylinder wall was visible in some places (Figure 30). Applying the mapping functions evaluated by DaVis to these pictures, global coordinates of these positions at the wall have been acquired. Then they have been used as centers of circles with the same diameter as the cylinder (at the right of Figure 30). The intersection of these plotted circles is the position of the center of the cylinder. Unfortunately, the center cannot be determined with a better precision than one millimeter.

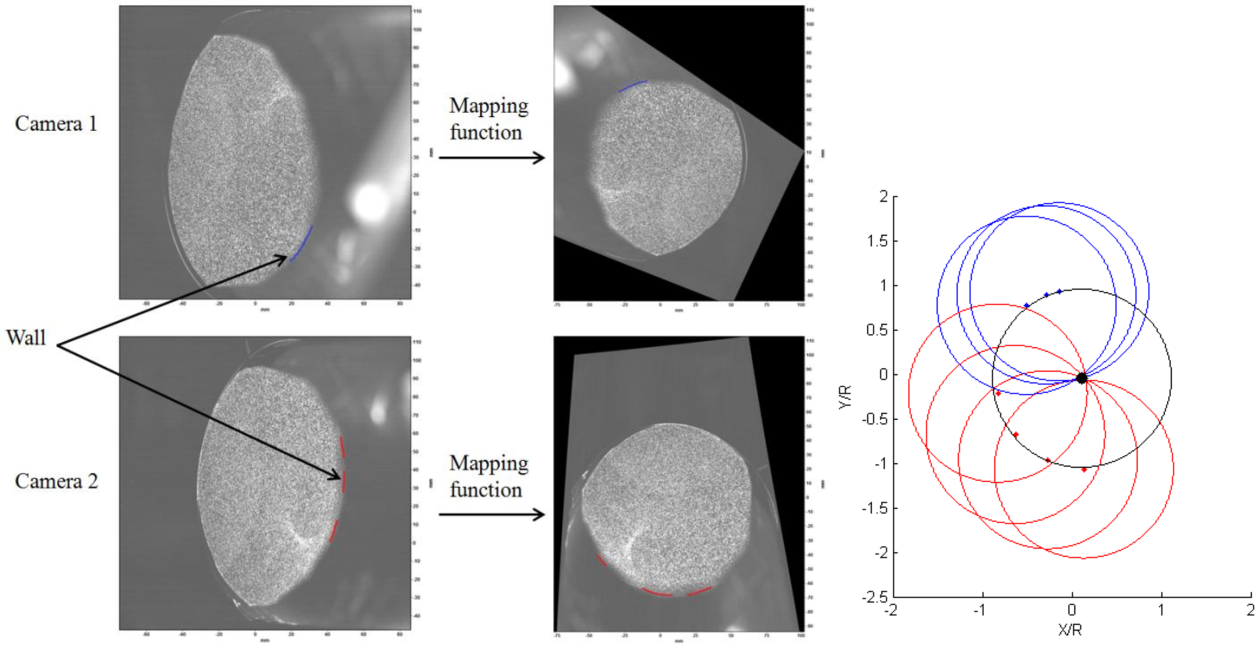

Figure 30. Method used to determine the center of the cylinder in the observed area.

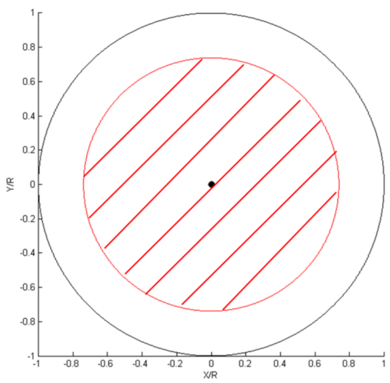

Figure 31. View of the cylinder from the top (black circle) and reduced area for which PIV data are available (hatched red circle).

The diameter of the cylinder is 130 mm but, as explained in the PIV chapter; to take pictures of the full horizontal plane was not possible since some blockage was used to hide reflections of the laser of the glass cylinder and that obstructed the field of view of the cameras. Finally the largest circular area centered on the cylinder center that could be studied had a diameter of 98mm. This area will usually be called the reduced surface and is depicted in Figure 31. Results from PIV has been plotted in this area except in indicated cases.

3.2. Analysis of the PIV results

3.1.1. The mean velocity field; Impact of inlet parameters on the flow motion

In a first step, the mean velocities evaluated with the ensemble averaged (eq. (1)) are studied to get an overview and understanding of the in-cylinder flow.

The normalized mean U_z velocity (velocity in the direction of the cylinder axis also called out-of-plane velocity) has been plotted with the streamlines of the in-plane mean motion. All cases from A_1 to C_3 are shown in appendix A.

In Figure 32, plots are shown for the cases A_3, B_3 and C_3 and therefore show the evolution of the out-of-plane velocity for different valve lifts.

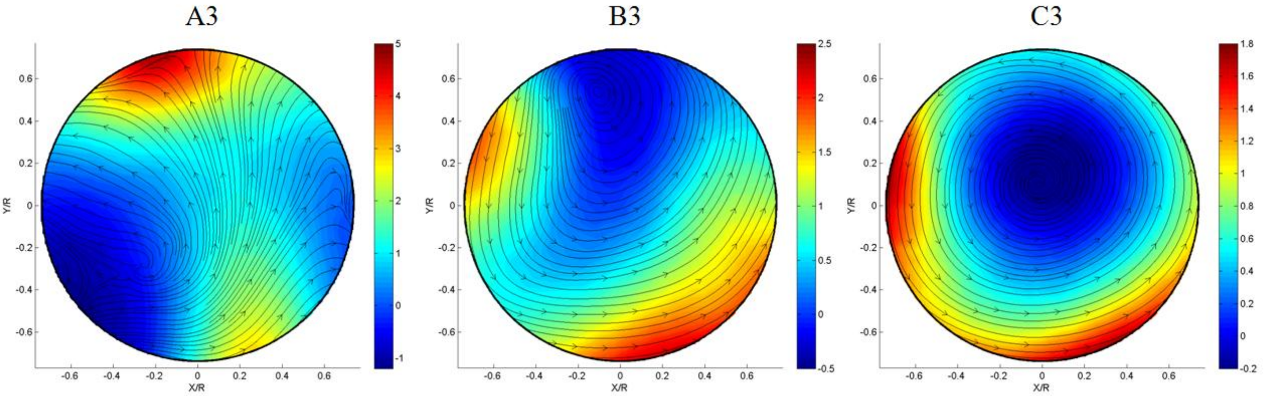

Figure 32. Plot of the normalized mean velocity component V_z (colors) and in-plane streamlines for cases A_3, B_3 and C_3.

It can be observed that the in-plane motion is totally different between the cases A_3 and B_3; the flow seems to separate in two different parts in the first case whereas a swirling motion appears over all the reduced surface in the second case. Differences are less visible but still important between cases B_3 and C_3; the swirling motion becomes more circular in C_3.

The same color scales couldn't be used for the three cases since the range of normalized U_z were too different from one case to another. The magnitude of the in-plane velocities has also been evaluated and the range of normalized velocities are listed for cases A_3, B_3 and C_3 in Table 3. When looking at the U_z range, it can be noticed that it is large for the case A_3 with a small valve lift; the range of U_z velocity decreases with an increase of valve lift. The reverse behavior is observed for the magnitude of in-plane velocities; the range is larger as the valve lift increases. The in-plane motion increases as the out-of-plane motion decreases.

The same study has been made comparing data for the same valve lift but with different pressure drops. As expected the influence of the pressure drop on the mean flow is negligible compared to the influence of the valve lift. This can be observed in the color plot of appendix A and on the evolution of the SR for the different cases with two inlet valves open in Figure 33. It shows that the SR and therefore the mean motion is much more dependent on the valve lift than on the pressure drop. This is highly desirable since it ensures the same flow structures for all engine speeds.

Case	Range of normalized U_z/U_{bulk}	Range of normalized magnitude of in-place velocities ($/U_{bulk}$)
A_3	5.6	1.0
B_3	2.3	1.8
C_3	2.0	2.0

Table 3. Thicknesses of velocity range for the normalized out-of-plan velocity and the normalized magnitude of in-plane velocity.

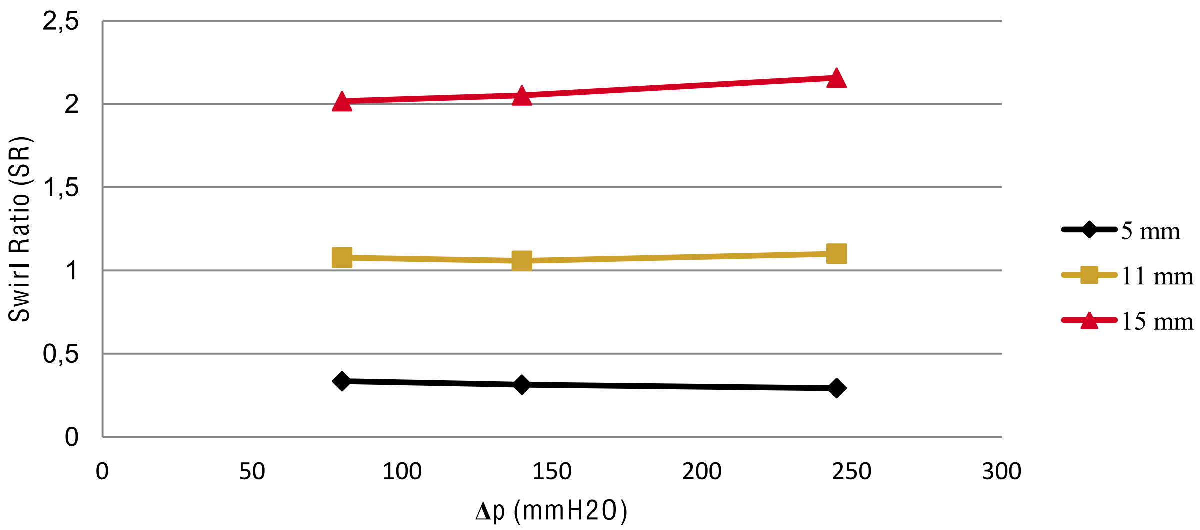

Figure 33. Evolution of the Swirl ratio as a function of the pressure drop and the valve lift.

3.1.2. Comparison with the solid body rotation theory

The theory of the solid body rotation is often used and compared to the motion of in-cylinder flow to evaluate rotations in a plane perpendicular to the cylinder axis. The azimuthal velocity of the experimental data has been studied to see if the in-plane motion could be considered more or less close to a rotating solid body. In case of solid body rotation, the azimuthal velocity at a position (x,y) around the center (x_0,y_0) is equal to the product between the angular velocity and the radius ($r = \sqrt{(x - x_0)^2 + (y - y_0)^2}$):

$$U_{azimuthal} = U_\theta = r \times \Omega$$

Since color plots are not always easy to evaluate, plots of the evolution of the azimuthal velocity along different lines in the horizontal plane passing through the center of the cylinder have been realized. The lines are visible at the top left in Figure 34. The azimuthal velocity has been calculated around the center of the cylinder and are plotted for the cases A_3, B_3 and C_3 (Figure 34).

It can be noticed that these plots confirm the previous conclusion that the range of in-plane velocities becomes larger when the valve lift increases.

For a small valve lift (A_3) the distribution of the azimuthal velocity (U_θ) is random; there is no correlation between its evolution along the different lines. This can also be observed in Figure 32; streamlines in case A_3 do not describe a swirling motion. When the valve lift increases (B_3), the evolution of U_θ along the four lines starts to be more linear but the coefficient of linearity is nevertheless different depending on the position in the reduced area. Finally at high valve lift (C_3), the linear behavior is increased and a constant coefficient of linearity could be found to link the evolution of

U_θ with the radius. Although there is a gap in the evolution of U_θ around the center of the cylinder (r=0) which indicates than the center of the swirl cannot be confused with the center of the cylinder.

Since cases A and B seems to have an azimuthal velocity too different from the one of a rotating solid body, this theory has therefore been applied only to the three cases C_1, C_2 and C_3 (with a 15mm valve lift).

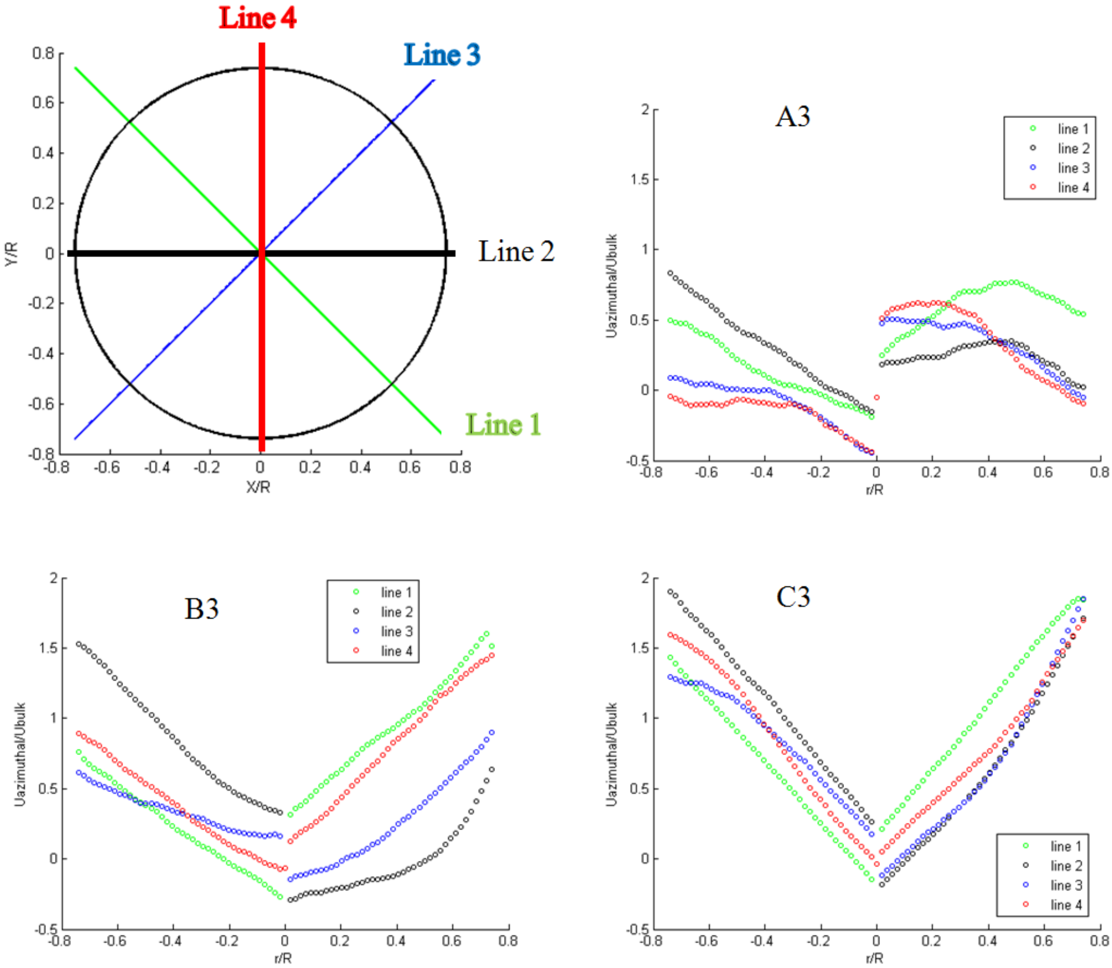

Figure 34. At the top left, lines along which the azimuthal velocities have been plotted. The three other plots represents the distribution of the azimuthal velocity calculated around the center of the cylinder along the four lines for cases A_3, B_3 and C_3.

An algorithm was developed that tried to fit a solid body rotation to the experimental data for different positions of the center over the reduced area. For each position, the RMS (standard deviation) over the surface between the angular velocity of the solid body rotation and the angular velocity of the mean flow field was evaluated. The center position (x_{sbr}, y_{sbr}) and the theoretical solid body with angular velocity of Ω_{sbr} ([rad/s]) giving the smallest RMS correspond to the closest one to the experimental data.

Results for case C_3 are shown in Figure 35. The two first plots (at the left and in the middle) have been realized using PIV data. At the left, there is the normalized azimuthal velocity computed around the center of the cylinder and in the middle the normalized azimuthal velocity is computed around the center found with the solid body rotation algorithm. The plot to the right is the normalized azimuthal velocity of the closest rotating solid body from the experimental data. It appeared that the center of the closest rotating solid body is the same as the center of the swirl (which can be evaluated with the streamlines in Figure 32).

Information about the corresponding solid body rotation for each experimental case can be read in Table 4. The distance of the solid body rotation from the center of the cylinder seems to be slightly different for the different pressure drops tested. However, the difference remains below 1mm and therefore is close to the precision than can be ensured by PIV measurements so this difference cannot be interpreted as a direct consequence of the increase of the pressure drop. The same remark can be made over the results for the normalized angular velocity; even if it seems to slightly increase with increasing pressure drop, it is not sure to be a direct consequence of the varying pressure drop. Once again, the engine speed doesn't seems to have an important influence on the in-cylinder flow. The strength of the swirl needs to be controlled in order to prevent problems of fuel sprays colliding, it is therefore interesting to know that this strength can vary during the opening of the valves but not as a function of the engine speed.

The RMS (standard deviation over the surface between the angular velocity of the solid body rotation and the angular velocity of the mean flow field) normalized by the bulk velocity between this closest theoretical solid body rotation and the experimental azimuthal velocity around the center of swirl is not superior to 0.15 for all cases C_1, C_2 and C_3. Comparing this RMS to the range of the azimuthal velocity in the reduced area, it is small enough to conclude that the theory of the solid body rotation is in good agreement with the experimental data of cases C_1, C_2 and C_3.

This study gives interesting results about the in-plane motion. However, since Stereo-PIV measurements have been made in this project, one can therefore say that this is actually an oversimplified way to describe the in-cylinder flow since the out-of-plane component of the velocity is not constant for all the reduced area (Figure 32): The gradient of the U_z velocity is too important to correspond to a solid body rotation, even if probable solid deformations are taken into account.

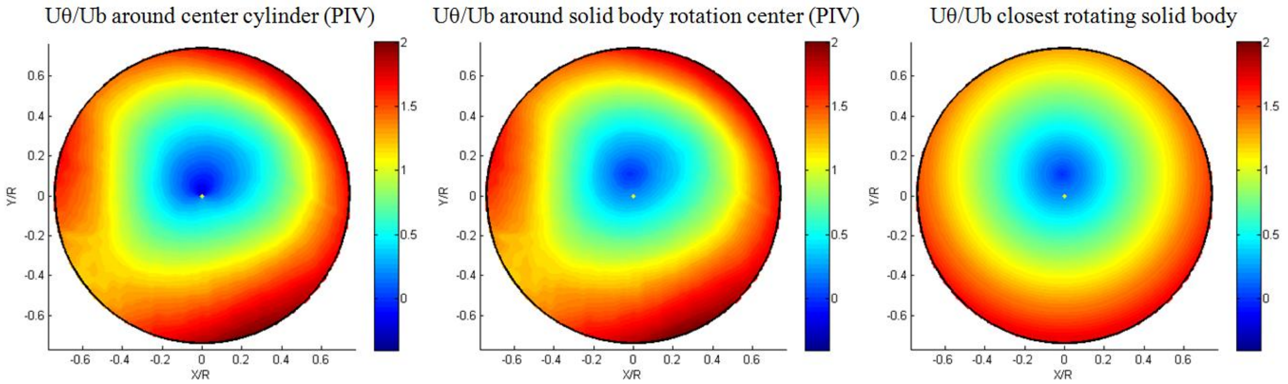

Figure 35. Plots of the normalized azimuthal velocity for the case C_3. The yellow dot represents the center of the cylinder.

Case	$(x_{sbr}\ ;\ y_{sbr})$ [mm]	$r_{sbr} = \sqrt{x_{sbr}^2 + y_{sbr}^2}$ [mm]	$\frac{\Omega_{sbr}}{U_{bulk}/R}$	RMS/U_{bulk}
C_1	(-0.4 ; 6.7)	6.7	4.0	0.15
C_2	(-0.1 ; 7.7)	7.7	4.1	0.16
C_3	(-0.8 ; 7)	7.0	4.2	0.15

Table 4. Information about the closest solid body rotation theories from the experimental data; center, distance from the center of the cylinder, normalized angular velocity and normalized RMS.

3.1.3. Study of the fluctuations looking at the instantaneous fields and the Reynolds stress tensor components

After obtaining a good overview of the mean flow field, it seems important to look at the instantaneous velocity fields as well as the Reynolds stress tensor components in order to understand the behavior of the fluctuations.

Instantaneous velocity fields

Looking at the instantaneous velocity fields (cases A_3, B_3 and C_3 in Figure 36) it can be noticed that the in-plane motion is much more random for case A_3 than for the two other cases and that scales of the motion are smaller than those observed in the two other cases. Actually, the largest scales can be observed for case C_3 when the valve lift is equal to 15mm, it seems that the swirling motion is already visible on the instantaneous velocity fields. One can also remark here again that the range of the out-of-plane velocity decreases when the valve lift increases.

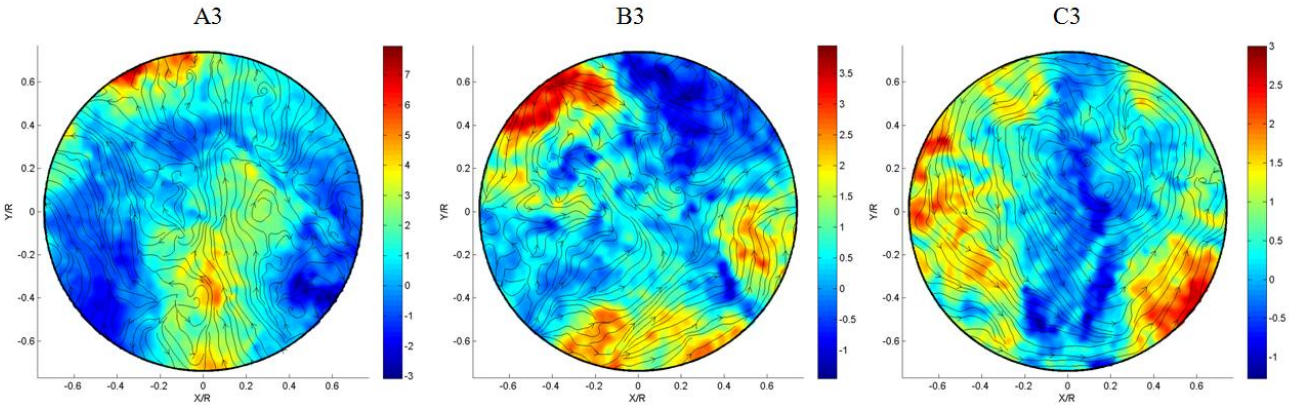

Figure 36. Randomly chosen instantaneous velocity fields for cases A_3, B_3 and C_3. Colors represents the normalized instantaneous velocity component v_z and streamlines represent the in-plane motion.

Here again comparison between cases tested with the same valve lift and different pressure drop seems to show that flow fields are not dependant on the pressure drop. No greater difference can be noticed between two instantaneous velocity fields taken with different pressure drop (same valve lift) than between two fields taken for the same case (same pressure drop and same valve lift).

Analysis of turbulence anisotropy

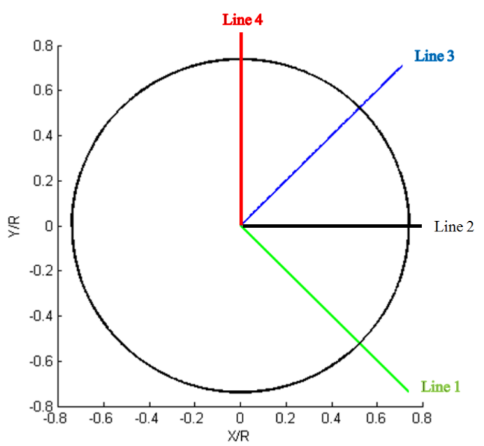

Figure 37. Four radius along which the evolution of the anisotropic invariants have been studied.

The invariant theory described in chapter 1 has been used to understand the dynamic of the fluctuating velocity field. To do so, the second and third invariant have been calculated at each position inside the reduced area using 1000 instantaneous velocity fields for each case.

Once again no noticeable differences were visible between cases with the same valve lift and different pressure drops which indicates that even the fluctuating motion of the flow field is not dependent on engine speed.

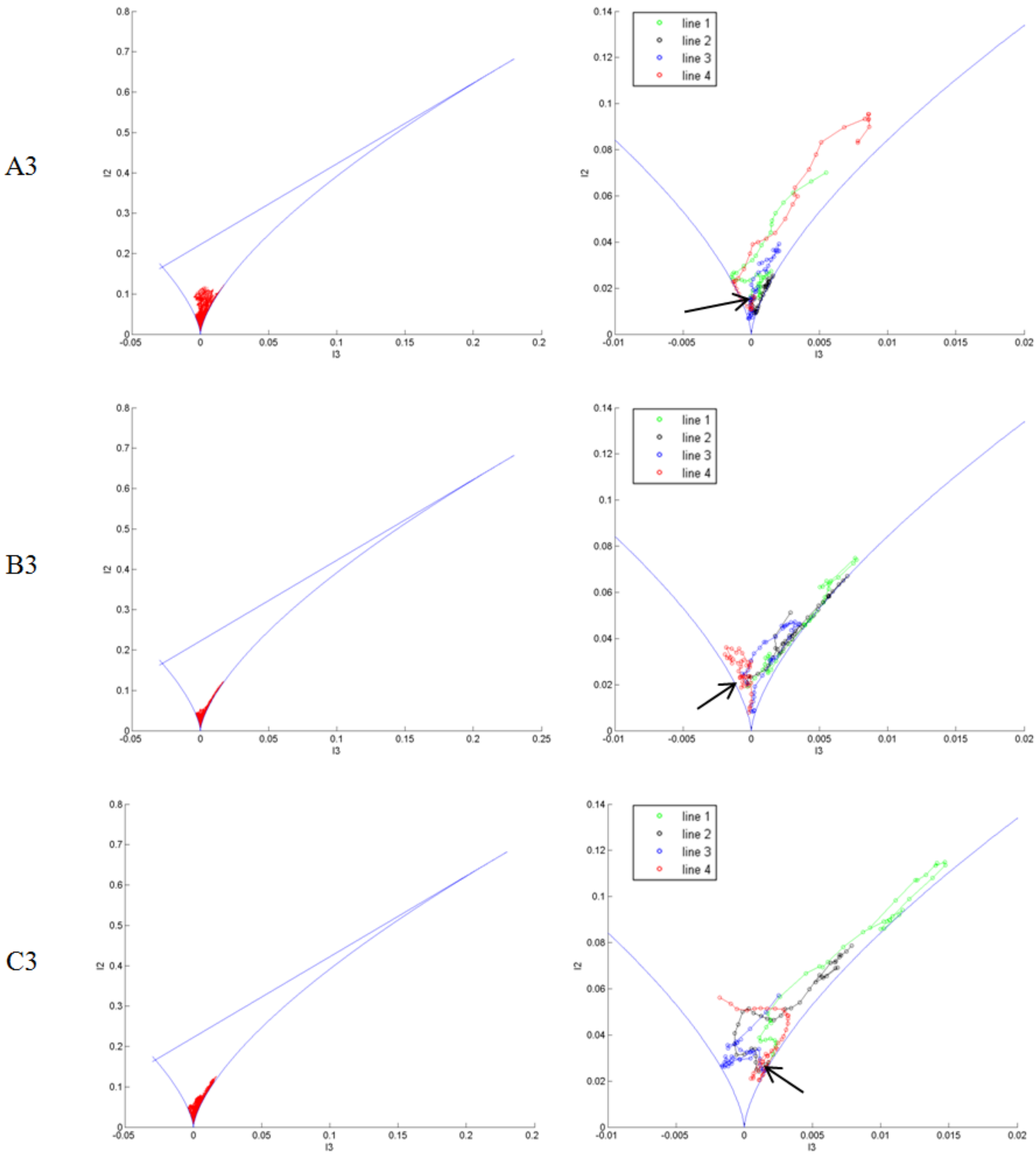

Figure 38. Lumley-Newman representation of the turbulence anisotropy for cases A_3, B_3 and C_3. Plots on the left represent all the data (in red) over the reduced area. To the right, a zoom is realized over the interesting part of the triangle and plots represent the invariants along different radius. The black arrows point at the invariants at the center of the cylinder.

Figure 38 shows plots of the anisotropy invariants for cases A_3, B_3 and C_3. Red plots on the left column represent the second invariant as a function of the third invariant calculated for all position inside the reduced area. It can be noticed that for all cases all the data (red dots) are contained inside the Lumley triangle. That means that the measurements probably are of good quality since there is no non-physical data. A clear difference can be seen for the case A_3, there is more values centered between the two limits corresponding to axisymmetric anisotropy. For the two other cases, the values are closer to the right boundary. That seems to indicates that even in the fluctuating field, a dominant motion is axisymmetric for a high valve lift but not for a small valve lift. For all cases, all the red dots are in a small region close to the lower corner, a zoom on this region has therefore been made for plots depicted in the right column.

Finally, even if the data are close to the isotropic region, it can be seen by zooming that there are no isotropic turbulence specially for the case of high valve lift. This conclusion is only available about scale motions that the PIV is able to identify but recalling that the step between each velocity vector is about 0.6mm, even quite small scales are observed here. This is an important information for the simulation of the in-cylinder flow since as explained in the part about turbulent flows, when using RANS simulation the Reynolds stress tensor is often assumed isotropic. The conclusion is thus that a LES model is useful when studying such flows.

3.1.4. Effects of the use of two intake valves on the mean flow

As explained in the 'plan of experiment' part, measurements have also been made by opening only one intake valve ; the valve number one in Figure 29. Tests B_1, and D_1 have been made with the same inlet conditions (valve lift of 11mm and pressure drop of 80 mmH_2O) as well as tests C_1 and D_2 (15mm of valve lift and 80 mmH_2O).

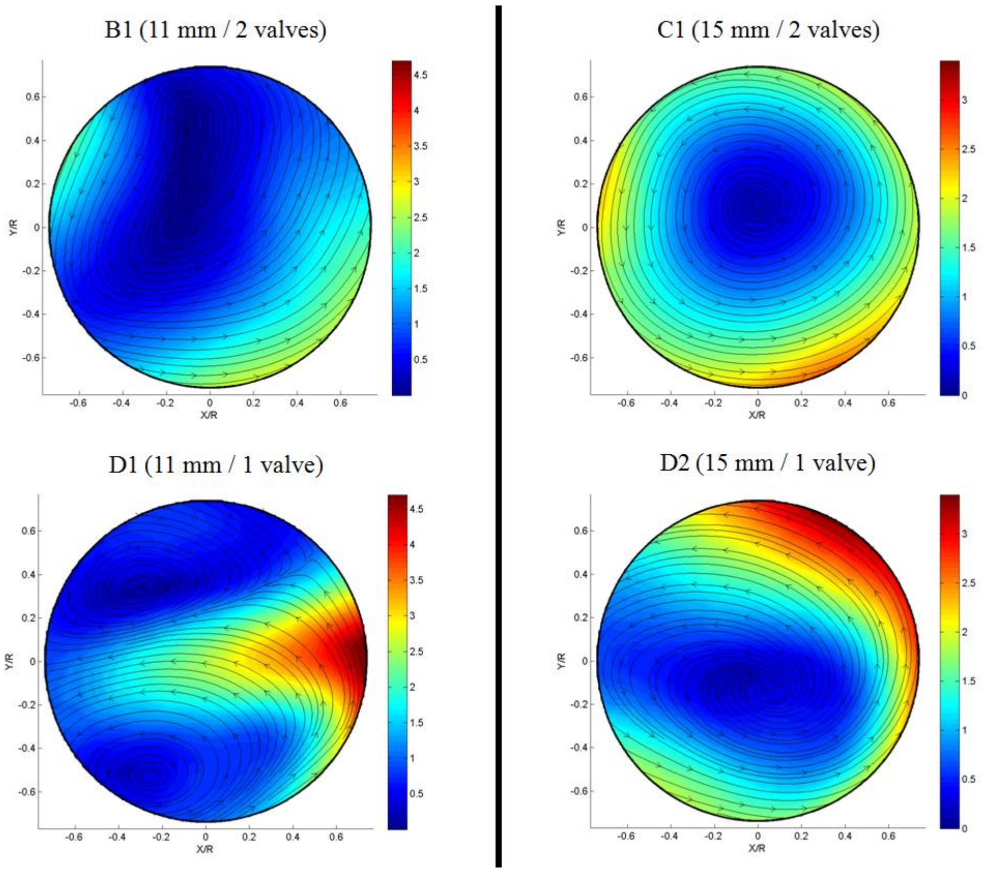

Figure 39. Results for the out-of-plane component normalized mean velocity Vz and in-plane streamlines for cases with one or two valves open (B_1, D_1, C_1 and D_2)

Results for the out-of-plane component of the normalized mean velocity and in-plane streamlines are shown in Figure 39 for the four cases. The first comment is that the range of this V_z component is clearly higher in cases for which one intake valve is open than for the corresponding case with two valves. However the volume flow is more or less the double in cases with two valves than the corresponding cases with one valve. This shows that the motion in the plane parallel to the cylinder axis is more important when only one valve is open than two. Moreover it can be noticed than the swirl motion is less visible in cases D_1 and D_2. In the first case, two different swirling motions in different directions appear (one clockwise and the other anticlockwise). In the second case, the one with a maximum valve lift, a swirling motion is visible but clearly less circular than when two intake valves are open.

These results confirm the fact that the design of ports and valves as well as the interaction of the flow with the cylinder wall are not the only actors of the swirl creation; the interaction of flow from the different open intake valves is also a reason for which the motion is important in the plane perpendicular to the cylinder axis as well as in the plane parallel to the axis. Moreover the swirling motion is established faster and becomes more circular thanks to the interaction between flow from the two valves which is also wishes since the fuel spray will be more homogeneously distributed with a circular swirl motion than with a swirling motion like the one of case D_2. However, the effect of the compression stroke on these swirls should be studied with meticulous care before drawing such conclusions.

Finally the results of SR calculation for the four cases are listed in Figure 40. It can be seen that the SR do not really change between cases with one or two intake valves open. However, as concluded before, the motion is clearly different. This is due to the fact that the SR is a quantity integrated for the whole area and shows the importance of using experimental methods like PIV to achieve information for the whole area.

	B_1 (11mm / 2 valves)	D_1 (15mm / 1 valve)	C_1 (15mm / 2 valves)	D_2 (15mm / 1 valve)
SR	1.1	1.0	2.0	2.0

Figure 40. Swirl Ration of the 4 cases B_1, D_1, C_1 and D_2.

3.2. Comparison of PIV measurements with LES simulations and honeycomb measurements

3.2.1. Qualitative study of the mean flow fields

There are results available from LES simulations for cases A_2, B_3 and C_3 that can be compared with the PIV measurements. Comparison between LES and PIV results of the radial, azimuthal and out-of-plane velocities for the three cases are shown in Figure 41, Figure 42 and Figure 43. Color scales used for the comparison of the same velocity component in the same case are the same for the PIV and the LES.

The results seems to be in qualitative good agreement, specially when looking at the normalized U_z velocity component. When looking at the radial and azimuthal components, gradients of velocities seems to be higher for the LES results than for the PIV results. For example the normalized azimuthal velocities for the case C_3, recalling that the PIV U_θ has a constant gradient along the radius of the cylinder, compatible with the solid body rotation, this kind of behavior does not seems to occur for the LES U_θ. An important increase of the LES U_θ is visible in the region close to the center of the cylinder;

U_θ varies from -0.6 to 1.5 along a normalized radius of 0.3, then the azimuthal velocity continues to increase but only from 1.5 to 2.1 for the outer region (normalized radius from 0.3 to 0.7). These differences are as small as they can be due to differences in the geometry between the PIV and LES. The complete geometry of the rig (Figure 5) has not been simulated since it was too complicated and would have needed an important number of cells to be meshed.

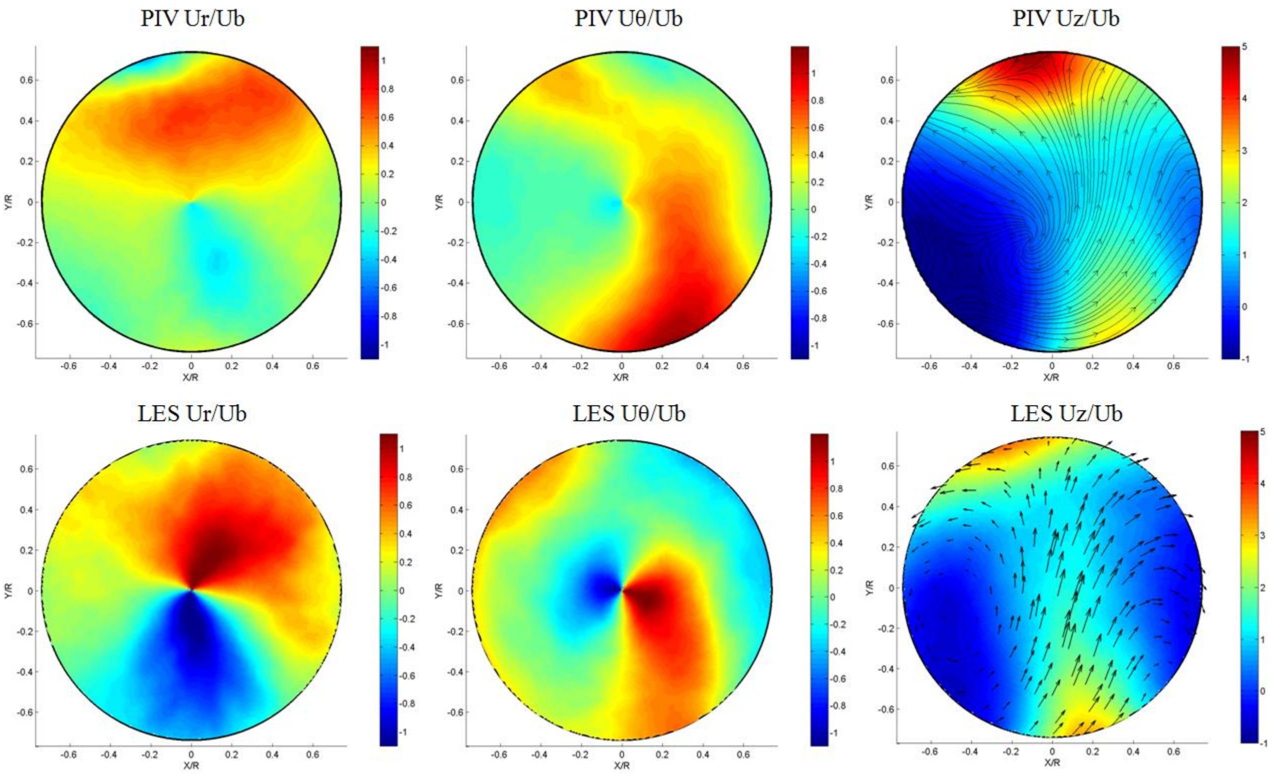

Figure 41. Comparison of radial, azimuthal and out-of-plane velocities between PIV measurements and LES simulations for case A_2.

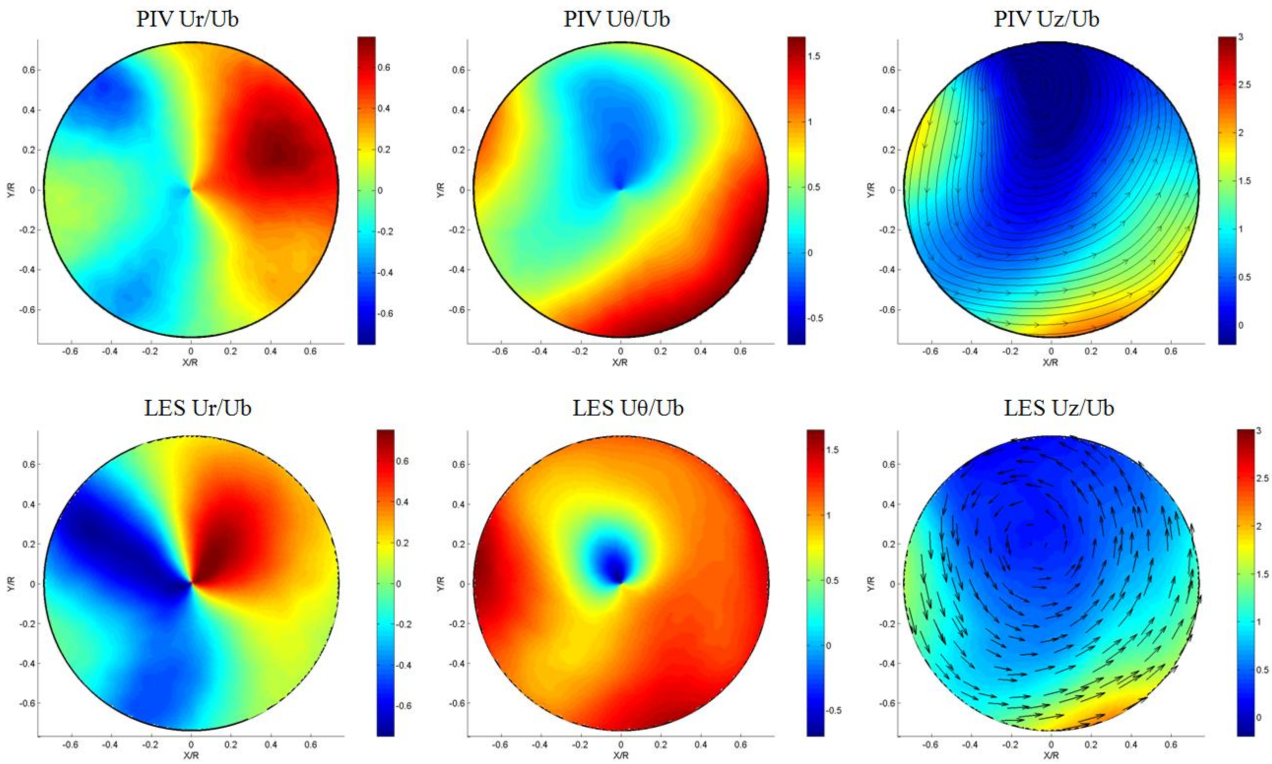

Figure 42. Comparison of radial, azimuthal and out-of-plane velocities between PIV measurements and LES simulations for case B_3.

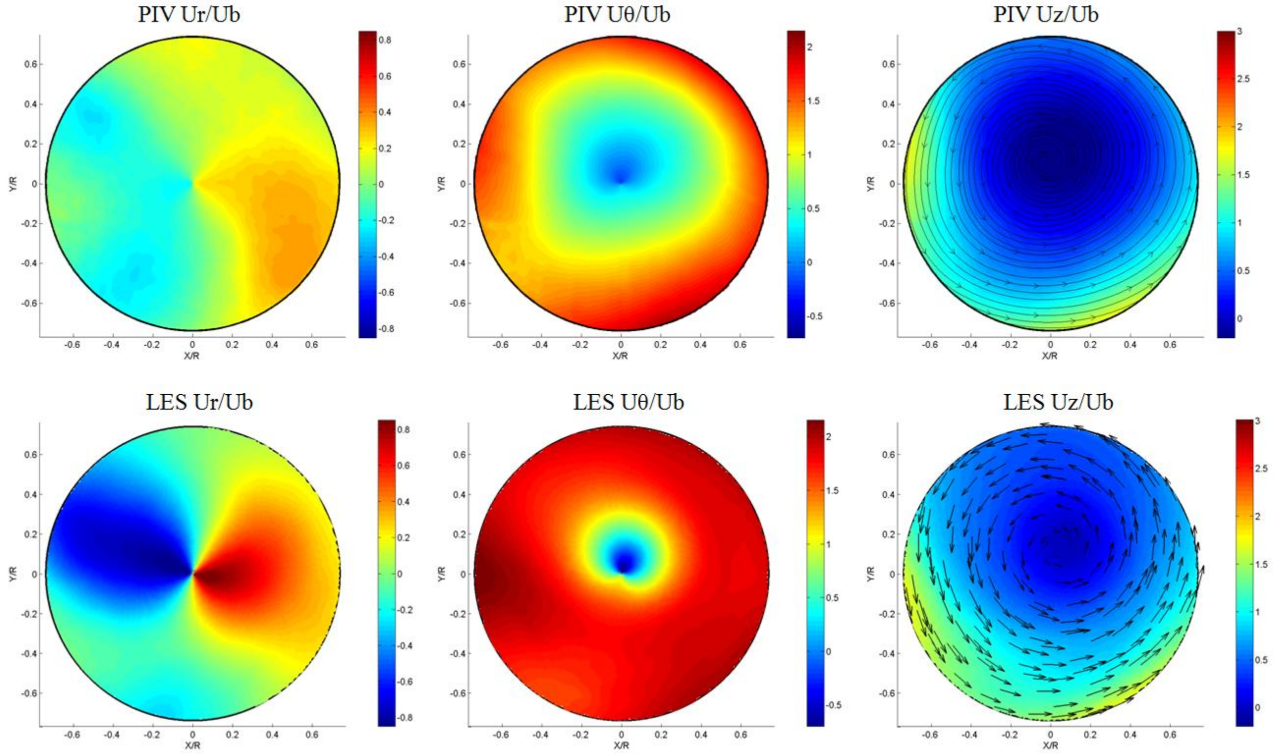

Figure 43. Comparison of radial, azimuthal and out-of-plane velocities between PIV measurements and LES simulations for case C_3.

3.2.2. Comparison of the swirl ratios and extrapolation of PIV results.

Another method to compare the results from the three different studies (PIV, LES and honeycomb measurement) was to compare the SR.

Unfortunately, as explained earlier, due to reflections of the laser on the cylinder, the cameras could not take pictures of the whole horizontal plane and therefore velocity fields over only a reduced area could be compared. The SR calculated over the reduced area for cases A_2, B_3 and C_3 are presented in Table 5 and are in good agreement even if the PIV seems to give slightly higher velocities than the LES simulations. This can be due to the fact that the method used to find the center of the cylinder and explained earlier has only a precision of 1mm and the areas compared between the experiments and the simulations can be slightly different.

In order to compare data for the whole area, results from the study of the solid body rotation have been used; the mean in-plane motion could be extrapolated in the area not visible on the PIV images using the angular velocity of the closest solid body rotation. A study has then been made of the evolution of the mean out-of-plane velocity along the radius to see if this component could also be extrapolated outside from the reduced area. The evolution of the U_z velocity component as a function of the radius has therefore been plotted as function of the radius for the case C_3 since it is the only case for which the azimuthal velocity component could be extrapolated. In Figure 44, all the values of the V_z velocity component from the Stereo-PIV experiments are plotted in red. Then an average along the radius has been made (blue curve). Finally, using a second order polynomial interpolation (green curve), the value of the mean out-of-plane velocity could be extrapolated outside from the reduced area and an extrapolated SR has been calculated for the whole horizontal area. Here the influence of the boundary layer at the wall has been ignored.

Data of the normalized SR calculated for the whole area is visible in the Table 5 and are close to each other confirming the fact that the three studies, PIV measurements, LES simulation and honeycomb measurements are in good agreement.

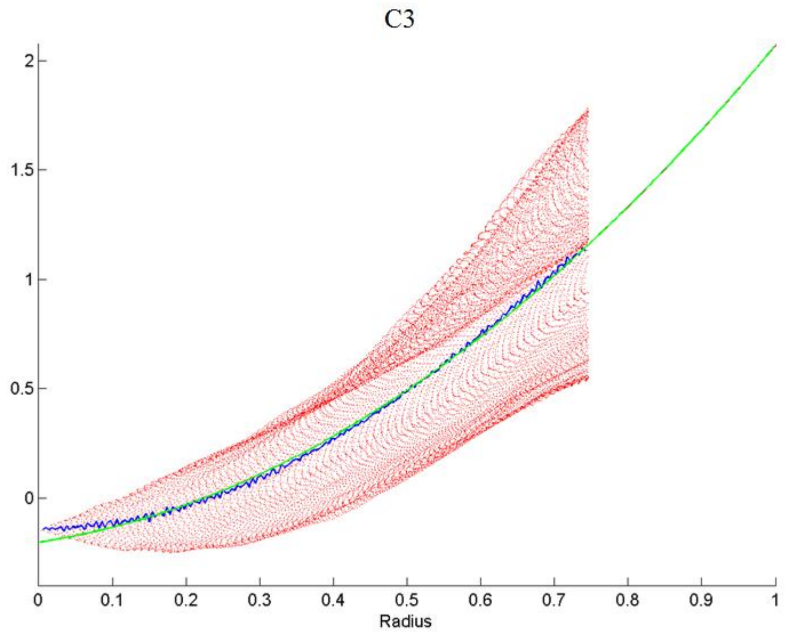

Figure 44. Evolution of the normalized out-of-plane velocity as a function of the radius. The red scatter data are the value of V_z velocity component inside the reduced area resulting from the Stereo-PIV measurements. The blue curve is the average of the scatter plot and the green curve results from the interpolation of the blue curve.

	Reduced area		Complete area		
Case	LES SR	PIV SR	Honeycomb SR	LES SR	PIV SR (extrapolation)
A_2	0.2	0.3	0.2	0.2	×
B_3	1.1	1.1	0.8	0.8	×
C_3	2.0	2.2	1.0	1.1	1.0

Table 5. Normalized Swirl Ratios (SR)

Conclusion

Summary of results

Thanks to the non-intrusive stereo-PIV technique, the three velocity components of the steady flow in a horizontal plane of the cylinder situated 165 mm below the cylinder head have been measured. In this thesis, different valves lifts and pressure drops across the flow bench have been tested.

All the results for the ensemble averaged velocity and the fluctuations show that the in-cylinder flow is strongly dependent on the valve-lift and so that strong variations occurs in the in-cylinder flow of a real engine since the valve lift evolves with the crank angle. When the valve lift is small, two different motions appear in the plane perpendicular to the cylinder axis, the flows from the two different valves do not seems to interact with each other. Then, when the valve lift increases, the interaction is stronger and only one swirling motion appears for the entire plane. This swirling motion becomes more and more circular with the increase of the valve lift until the two-dimensional in-plane motion becomes highly comparable to a two-dimensional solid body rotation. As expected, the center of the swirl does not coincide with the center of the cylinder probably because of the tumble affect. However, results for the different pressure drops applied through the flow bench did not show any remarkable differences. It means that the in-cylinder flow motion is only weekly dependent on the engine speed. This is highly desirable since it means that if valves and ports are chosen for their efficiency to improve the fuel/air mixture, this efficiency will be kept whatever the speed of the engine.

The study of the anisotropic invariants showed that even though the turbulence is fairly close to the isotropic limit, it cannot be considered as isotropic. The choice of LES simulation is therefore relevant and seemed in a good agreement with the PIV results even if some disparities could be observed partly due to differences in the geometry downstream of the cylinder. Results for the swirl ratio, SR, using the three methods, PIV, LES and honeycomb measurements have been compared and are close but the study of the effect of opening only one intake valve showed the importance to use experimental methods for which values for the complete area or volume are available. Due to its complexity, integral parameters are far away from being sufficient to describe the in-cylinder flow.

Future work

A Proper Orthogonal Decomposition (POD) as Lumley proposed in (LUMLEY, 1967) could be applied to the set of data. This method has given interesting results in many in-cylinder PIV studies and could bring more information about the flow (FOGLEMAN, LUMLEY, REMPFER, & HAWORTH, 2004), (KEROMNES, DUJOL, & GUIBERT, 2010). The POD has actually been tested using the DaVis software during this project, modes seemed correct and the amount of energy in each of them showed a good convergence. However, the energy in the first mode was only of 10% due to the fact that the mean flow is first subtracted from all modes. DaVis being a commercial software it is not possible to know exactly which code is applied to realize this POD and therefore it could be more interesting to realize all the decomposition oneself.

The PIV setup could be used to study the flow in a plan perpendicular to the cylinder axis closer to the valves in order to study the way the flow from each valve interact with each others. A lot of laser reflections will have to be corrected but to paint the parts of the cylinder head with the fluorescent paint could probably solve many of them. It could also be interesting to study the tumble motion with the PIV but the difficulty is to find in which plane parallel to the cylinder axis this motion occurs, this plane is probably not the same for all the valve lifts.

The results shown in this report are based on just a small part of all the available data. In total more than 1Tb of experimental data was collected and there is plenty of room for further analysis which probably will provide further insight into this kind of flows.

Appendices

A. Normalized mean V_z velocity (colors) and in-plane streamlines

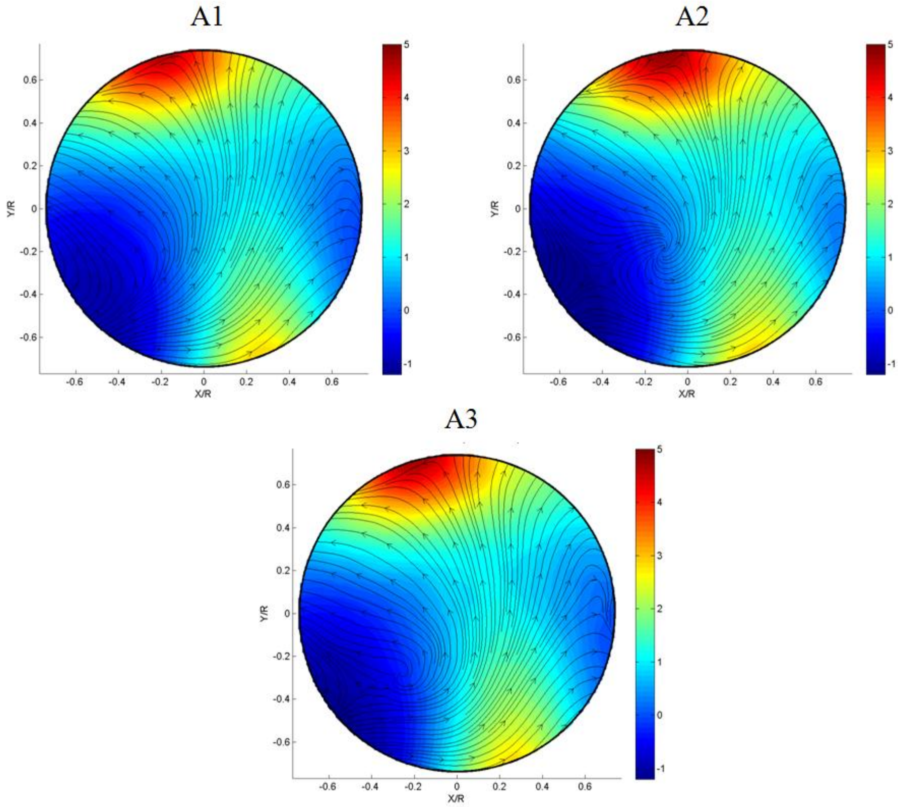

Figure 45. Plot of the normalized V_z velocity (colors) and in-plane streamlines for cases A_1, A_2 and A_3.

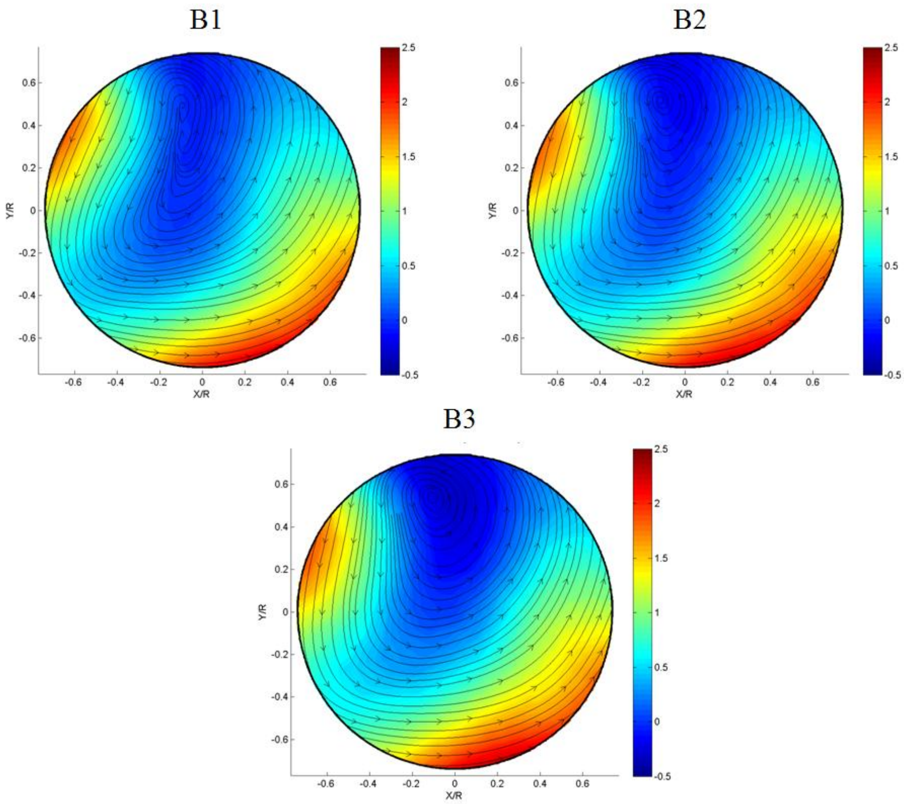

Figure 46. Plot of the normalized V_z velocity (colors) and in-plane streamlines for cases B_1, B_2 and B_3.

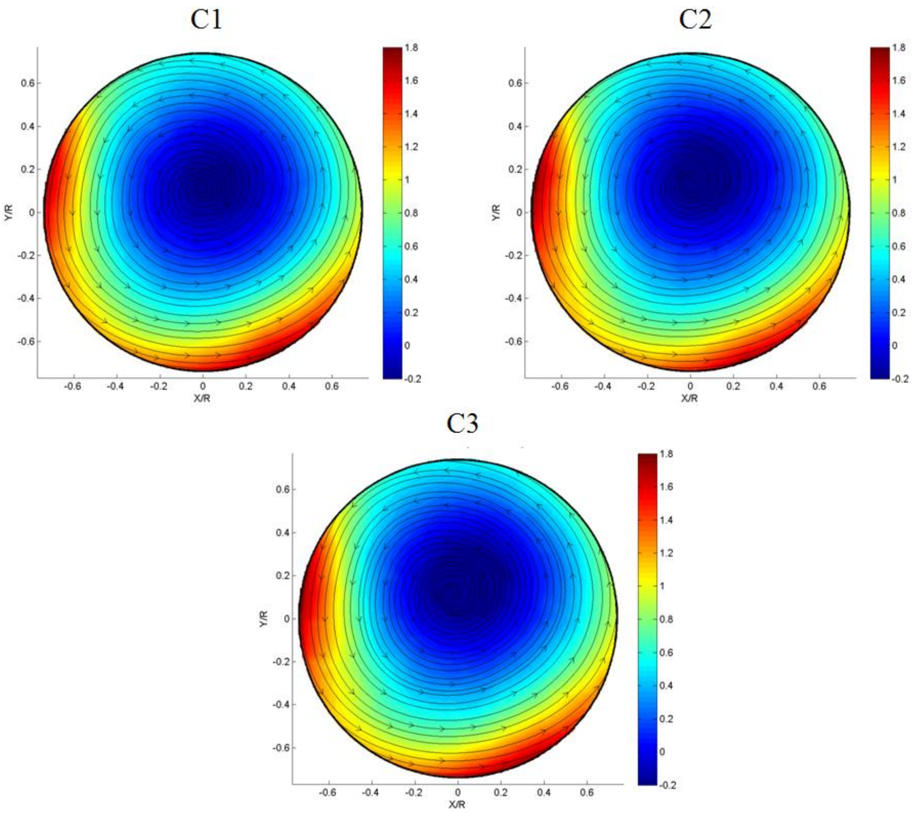

Figure 47. Plot of the normalized V_z velocity (colors) and in-plane streamlines for cases C_1, C_2 and C_3.

References

ALGER, T., MCGEE, J., GALLANT, E., & WOLLDRIDGE, S. (2004). PIV in-cylinder flow measurements of swirl and the effect of combustion chamber design. *SAE Technical Paper*.

ARGACHOY, C., & PIMENTA, A. P. (2005). Phenomenological model of particulate matter emission from direct injection Diesel engines. *ABCM*, *XXVII*, 266-273.

CHRISTENSEN, K. T. (2004). The influence of peak-locking errors on turbulence statistics computed from PIV ensembles. *Experiments in Fluids*, *36*, 484-497.

COSADIA, I., BORÉE, J., CHARNAY, G., & DUMONT, P. (2006). Cyclic variations of the swirling flow in a diesel transparent engine. *Experiments in Fluids*, *41*, 115-134.

DEMBINSKI, H. W. (2011). Optical study of swirl during combustion in a CI engine with different injection pressures and swirl ratios compared with calculations. *SAE International*, *2012-01-0682*.

Diesel Engine Fundamentals. (n.d.). Retrieved from DieselNet: http://www.dieselnet.com/tg.php

ESCUDIÉ, R., & LINÉ, A. (2005). Analysis of turbulence anisotropy in a mixing tank. *Chemical Engineering Science*, *61*, 2771-2779.

FEI, R., & MERZKIRCH, W. (2004). Investigations of the measurement accuracy of stereo particle image velocimetry. *Experiments in Fluids*, *37*, 559-565.

FOGLEMAN, M., LUMLEY, J., REMPFER, D., & HAWORTH, D. (2004). Appllication of the proper orthogonal decomposition to datasets of internal combustion engine flows. *Journal of Turbulence*, *5*, *N23*.

Four-stroke diesel engine. (n.d.). Retrieved from Encyclopedia Britannica: http://www.britannica.com/EBchecked/media/19423/Four-stroke-diesel-engine-The-typical-sequence-of-cycle-events

GURLEK, C., & SAHIN, B. (2010). Particle image velocimetry studies around a rectangular body close to a plane wall. *Flow Measurement and Instrumentation*, *21* (3), 322–329.

HEIM, D., & GHANDHI, J. (2011). A detailed study of in-cylinder flow and turbulence using PIV. *SAE International*.

HEYWOOD, J. B. (1988). *Internal combustion engine fundamentals.* McGraw-Hill.

HONKANEN, M., & NOBACH, H. (2005). Background extraction from double-frame PIV images. *Experiments in Fluids*, *38*, 348-362.

INTERNATIONAL ENERGY AGENCY. (2011). *CO2 emissions from fuel combustion, highlights.*

KEROMNES, A., DUJOL, C., & GUIBERT, P. (2010). Aerodynamic control inside an internal combustion engine. *Measurement Science and Technology*, *21*.

KIGER, K. Introduction of particle image velocimetry. *Burgers program for fluid dynamics, Turbulence school.* The A. James Clark school of engineering, College Park, Maryland.

LAMARQUE, N., ZOPPÉ, B., LEBAIGUE, O., DOLIAS, Y., BERTRAND, M., & DUCORS, F. (2010). Large-eddy simulation of the turbulent free-surface flow in an unbaffled stirred tank reactor. *Chemical Engineering Science*, *65*, 4307-4322.

LAVISION GmbH. (2011). *LaVision PIV-seminar 2011.* Göttingen, Germany.

LAVISION GmbH. (2010). *DaVis PIV-Manual, FlowMaster.* Göttingen, Germany.

LAVISION GmbH. (2011). *DaVis PIV-Manual, Imaging tools.* Göttingen, Germany.

LINDGREN, B. (2003). *Formler för beräkning av flödesparametrar i kanalutvärderingsprogrammet "SNURR".* Beskrivning, NMEG.

LINDGREN, B. (2004). *Intruktion för körning av blåsbänk B1&B3.* Instruction, NMEG.

LINDQUIST, C. (2005). *Thèse de doctorat. Contrôle électromagnétique d'écoulements. Etude expérimentale et numérique sur le forcage d'écoulements intialement au repos et en tunnel hydraudynamique.* Université Joseph Fourier, Grenoble.

LUMLEY, J. L. (1978). Computational modelling of turbulent flows. *Advanced Applied Mechanics , 18*, 123-176.

LUMLEY, J. L. (1967). The structure of inhomogeneous turbulence. Proceedings Atmospheric turbulence and radio-wave propagation. (Nauka, Ed.) 166-178.

LUMLEY, J. L., & NEWMANN, G. R. (1977). The return to isotropy of homogeneous turbulence. *Journal of Fluid Mechanics , 82*, 161-178.

MURALI KRISHNA, B., & MALLIKARJUNA, J. M. (2011). Effect of engine speed on in-cylinder tumble flows in a motored internal combustion engine - an experimental investigation using particle image velocimetry. *Journal of Applied Fluid Mechanics , 4* (1), 1-14.

NORDGREN, H., HILDINGSSON, L., JOHANSSON, B., DAHLÉN, L., & KONSTANZER, D. (2003). Comparison between in-cylinder PIV measurements, CFD simulations and steady-flow impulse torque swirl meter measurements. *SAE Technical Paper* .

OISHI, M., KINOSHITA, H., FUJII, T., & OSHIMA, M. (2011). Simultaneous measurement of internal and surrounding flows of a moving droplet using multicolour confocal micro-particle image velocimetry (micro-PIV). *Measurement Science and Technology , 22* (10).

PASHTRAPANSKA, M., JOVANOVIC, J., LIENHART, H., & DURST, F. (2006). Turbulence measurements in a swirling pipe flow. *Experiments in Fluids , 41*, 813-827.

POPE, S. B. (2000). *Turbulent flows.* Cambridge, UK: Cambridge University Press.

PRASAD, A. (2000). Stereoscopic particle image velocimetry. *Experiments in Fluids , 29*, 103-116.

RAFFEL, M., WILLER, C. E., WERELEY, S. T., & KOMPENHANS, J. (2007). *Particle image velocimetry, a practicle guide* (Second edition ed.). Springer.

REUS, D., ADRIAN, R., LANDRETH, C., FRENCH, D., & FANSLER, T. (1989). Instantaneous planar measurements of velocity and large-scale vorticity and strain rate in an engine using particle image velocimetry. *SAE Technical Papers , 890616.*

Scheimpflug principle. (n.d.). Retrieved from WIKIPEDIA: http://www.en.wikipedia.org/wiki/Scheimpflug_principle

SIMONSEN, A. J., & KROGSTAD, P.-Å. (2005). Turbulent stress invariant analysis: clarification of existing terminology. *Physics of Fluids , 17.*

STANISLAS, M., OKAMOTO, K., & KÄHLER, C. (2003). Main results of the First international PIV challenge. *Measurement Science and Technology , 14*, R63-R89.

Valves and Ports in Four-Stroke Engines. (n.d.). Retrieved from DieselNet: http://www.dieselnet.com

WIENEKEN, B. (2005). Stereo-PIV using self-calibration on particle images. *Experiments in Fluids , 39*, 267-280.